# One-Step Solid-State Mechanochemical Synthesis of Metal Chalcogenides as a Perspecitve Alternative to Traditional Preparation Routes


**Matej Baláž, Martin Stahorský, Peter Baláž, Erika Dutková, and Marcela Achimovičová**

## Abbreviations

| | |
|---|---|
| CFTS | Copper iron tin sulfide |
| CTS | Copper tin sulfide |
| CZTS | Copper zinc tin sulfide |
| ED | Electron diffraction |
| EDS | Energy-dispersive X-ray spectroscopy |
| ESM | Eccentric vibratory mill |
| FFT | Fast Fourier transform |
| HRTEM | High-resolution transmission electron microscopy |
| ICDD-PDF | International Centre for Diffraction Data–Powder Diffraction File |
| INCOME | International Conference on Mechanochemistry |
| IUPAC | International Union of Pure and Applied Chemistry |
| JCPDS | Joint Committee on Powder Diffraction Standards |
| SAED | Selected area electron diffraction |
| $S_{BET}$ | Brunauer-Emmett-Teller specific surface area |
| SEM | Scanning electron microscopy |
| TEM | Transmission electron microscopy |
| UV-Vis | Ultraviolet-visible |
| XRD | X-ray diffraction |

M. Baláž (✉) · M. Stahorský · P. Baláž · E. Dutková · M. Achimovičová
Institute of Geotechnics, Slovak Academy of Sciences, Košice, Slovakia
e-mail: balazm@saske.sk



F. I. Ezema et al. (eds.), *Chemically Deposited Metal Chalcogenide-based Carbon Composites for Versatile Applications*, https://doi.org/10.1007/978-3-031-23401-9_12

# 1 Introduction to Mechanochemistry

Mechanochemistry is defined as a branch of chemistry that is concerned with chemical and physicochemical changes of substances of all states of aggregation due to the influence of mechanical energy [1]. According to the International Union of Pure and Applied Chemistry (IUPAC), which also recognizes it, a mechanochemical reaction is a chemical reaction that is induced by the direct absorption of mechanical energy [2]. In simple words, it is an alternative method to the traditional solution-based chemistry due to the availability to perform chemical reactions completely in solid state in the absence of toxic solvents and external elevation of temperature and pressure. It was defined as a separate research field at the beginning of twentieth century [3] and has been proven to be applicable in distinct research areas since then, as it is demonstrated in Fig. 1. Its applicability is mostly in chemistry, materials science, and environmental sciences.

## *1.1 High-Energy Milling*

High-energy milling is a tool to perform mechanochemical reactions. Apart from conventional ball milling that delivers only limited amount of energy mainly to reduce the particle size of the treated material, additional effects like mechanical activation and defect formation are observed by applying high-energy mills. Conventional ball milling also most often does not lead to the occurrence of chemical reaction. Today, there is a number of high-energy ball mills that efficiently deliver the energy to the treated powders (examples are shown in Fig. 2). For less energy-demanding reactions like organic ones, mixer or shaker mills are usually employed (Fig. 2b). The effect of milling is achieved by an intensive shaking from one side to the other, and the milling chambers usually have the cylindrical shape with a

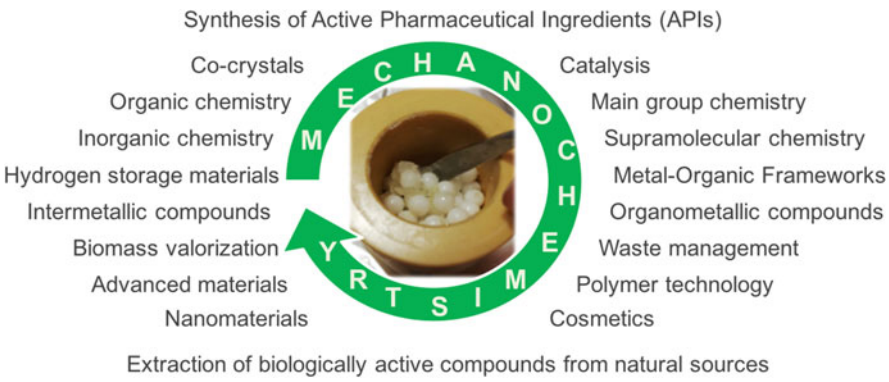


**Fig. 1** Diverse applications of mechanochemistry [4]

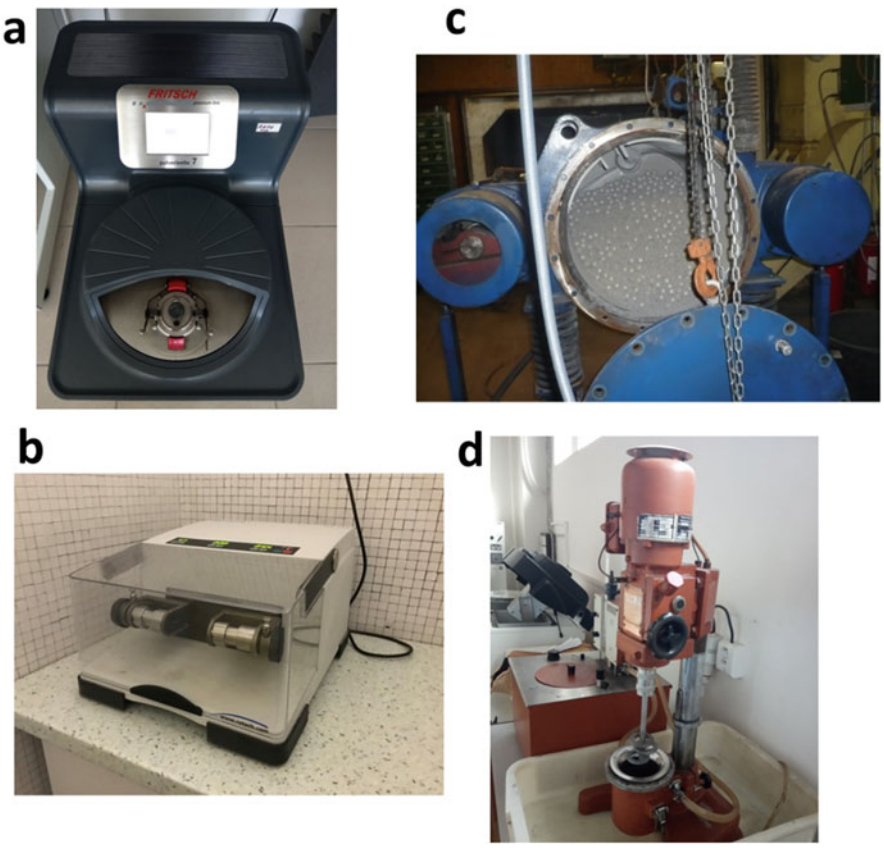


**Fig. 2** Examples of high-energy mills used for mechanochemical processes: (**a**) planetary ball mill, (**b**) electric shaker mill, (**c**) eccentric vibratory mill, (**d**) attrition mill. (Adapted from Springer Nature Customer Service Centre GmbH: Springer Nature [5] [COPYRIGHT] (2021))

volume of up to 20 mL. However, to perform more energy-demanding inorganic synthesis, the planetary ball mills where the milling chamber is located on the disc and is being intensively rotated to the one side, while the disc is being rotated to the other one, are being used (Fig. 2a). The volumes of the chambers used in the planetary ball mills are usually up to 500 mL. Shaker/mixer and planetary mills are exhaustively applied for the lab-scale experiments, but they are not suitable for implementation on a larger scale. In order to scale up mechanochemical reactions, eccentric vibratory (Fig. 2c) or attrition mills (Fig. 2d) can be applied.

There are plenty of experimental conditions that can be changed when performing the high-energy milling treatment. The most common ones are presented in Fig. 3. Depending on the treated material, different conditions might be suitable. One of the greatest challenges in mechanochemistry is the abrasion of milling media, which contaminates the product. This problem can be overcome, or at least

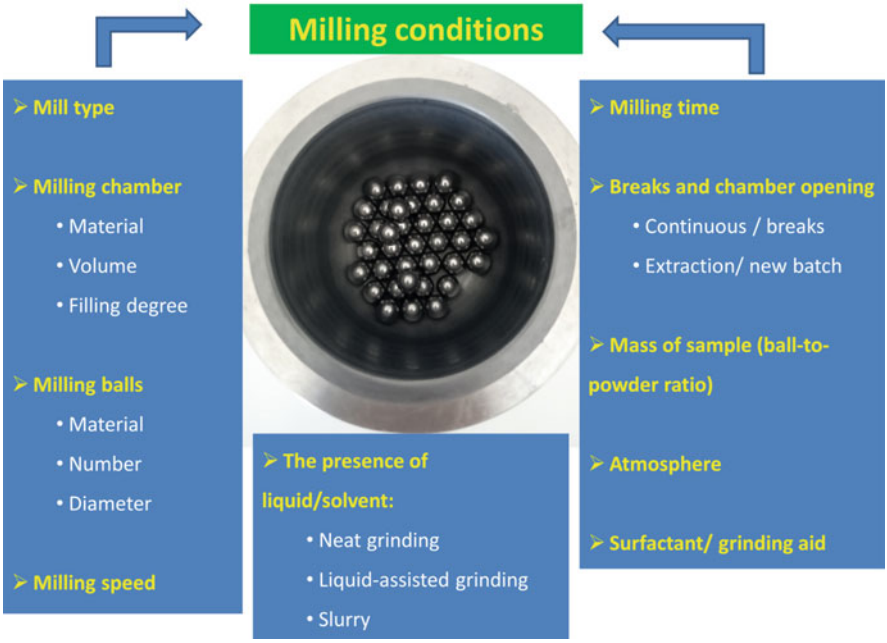


**Fig. 3** Most commonly changed experimental conditions during high-energy milling. (Reprinted by permission from Springer Nature Customer Service Centre GmbH: Springer Nature [5] [COPYRIGHT] (2021))

significantly reduced, by changing the conditions like the material of milling media, revolution speed, or using the grinding aids.

The high-energy milling treatment of the powders can lead to two scenarios. Either just physicochemical characteristics of the treated solids (such as particle size or specific surface area) are changed, however, no clear chemical change is observed. In this case, the process can be defined as mechanical activation. On the other hand, when a clear chemical change occurs, we are talking about mechanochemical reaction. To illustrate this difference, Fig. 4 is shown. The two processes can take place in one system, and mechanical activation of the reactants is often necessary before they undergo the mechanochemical reaction.

In most research groups working with mechanochemistry around the world, it is being tested as an alternative to the procedures that are already established there (as an example, performing organic reactions via the traditional solution-based methods versus mechanochemical one can be mentioned). However, the authors of this chapter are part of the department, where mechanochemistry is the main research focus and the high-energy milling is being applied for the processing of a wide variety of materials (Fig. 5).

As it can be seen, one of the main research directions is the mechanochemical synthesis of chalcogenides. This has been a permanent agenda at the Department as manifested in the reviews [7, 8] and monographs from the years 2000–2021

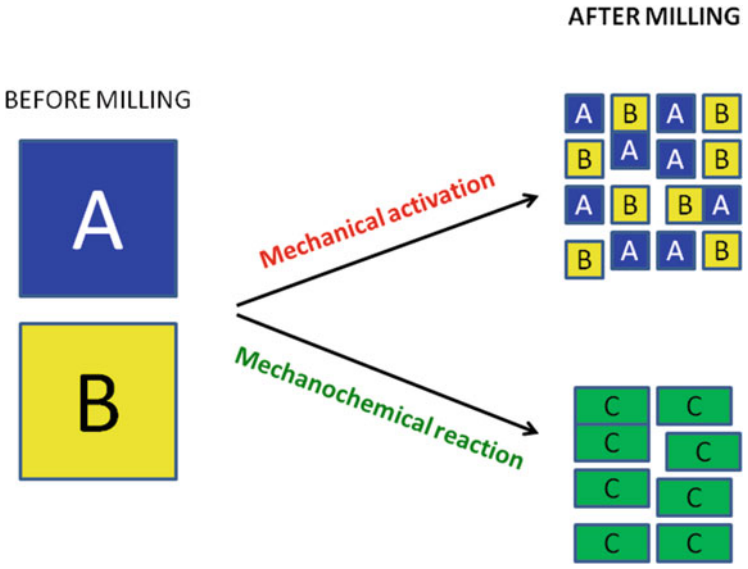


**Fig. 4** Schematic illustration showing the difference between mechanical activation and mechanochemical reaction (A, B- reactants, C- product of mechanochemical reaction). (Reprinted by permission from Springer Nature Customer Service Centre GmbH: Springer Nature [5] [COPYRIGHT] (2021))

published by the authors of this chapter [5, 9, 10]. In the present work, the overview of recent works of our research group from the year 2018 is provided. This is complemented by providing overview tables on the mechanochemical syntheses of chalcogenides by other research groups around the world. As the mechanochemical synthesis can also be performed in the scale-up fashion, the text is subdivided into a lab-scale and scalable synthesis. Further structuring is based on the chemical composition of chalcogenides, namely to binary, ternary, and quaternary ones.

## 2 Laboratory-Scale Mechanochemical Synthesis of Chalcogenides

The simplicity of mechanochemical synthesis of chalcogenides in comparison with other methods can be well demonstrated by the fact that just high-energy milling of the solid precursors is satisfactory to obtain nanocrystalline products [8]. Most often, two methodologies are applied; either the elements or compounds are used as precursors. The second option became preferred with time, as the obtained nanoparticles are usually smaller and thus more suitable for advanced applications, for example, as quantum dots. The principle of the two methodologies is demonstrated in the example of sulfides synthesis below (Fig. 6). The concept

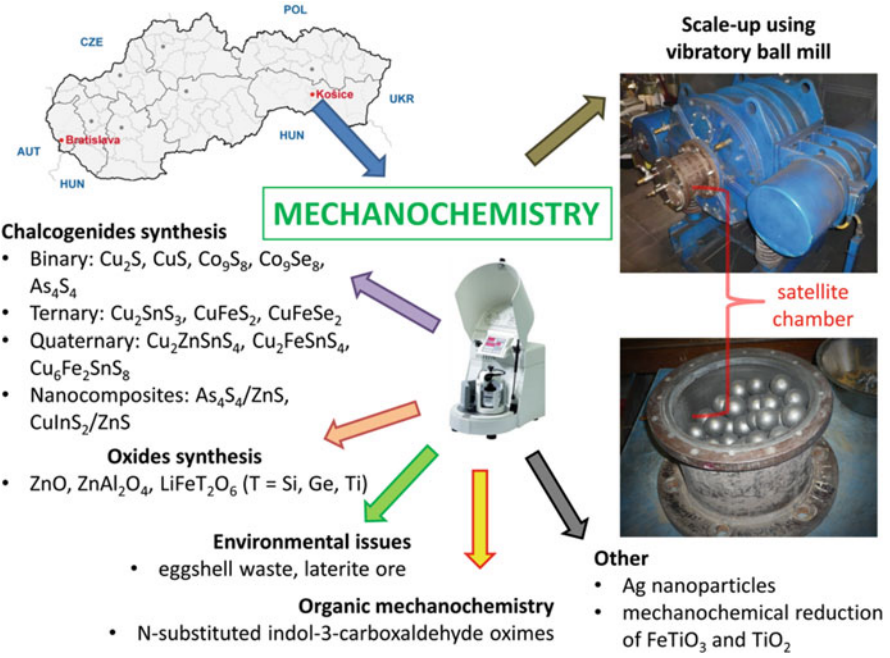


**Fig. 5** Variety of research activities being performed at the Department of Mechanochemistry, Institute of Geotechnics, Slovak Academy of Sciences in Košice, Slovakia. (Reprinted from [6], Copyright (2020), with permission from Elsevier)

of using metal acetate and sodium sulfide as the precursor of metal and sulfur, respectively, has been introduced by the research group of the authors of this chapter already in [11]. This synthetic pathway is sometimes referred to as a wet one because sodium sulfide is used as nonahydrate and the resulting reaction mixture often resembles a slurry. As a side-product, sodium acetate, which can be easily washed out, is formed.

## 3 Binary Systems

### *3.1 Cobalt Pentlandite, $Co_9S_8$*

$Co_9S_8$ nanoparticles from cobalt and sulfur in stoichiometric ratio in a planetary ball mill in an inert atmosphere were successfully prepared via mechanochemical synthesis in [12]. The cubic $Co_9S_8$ nanoparticles were nanocrystalline with crystallite size of about 16 nm, as confirmed by both Rietveld analysis and transmission electron microscopy. They consist of nanocrystals closely aggregated into spherical-like objects. The kinetics reaction studied by X-ray diffraction (XRD) is depicted

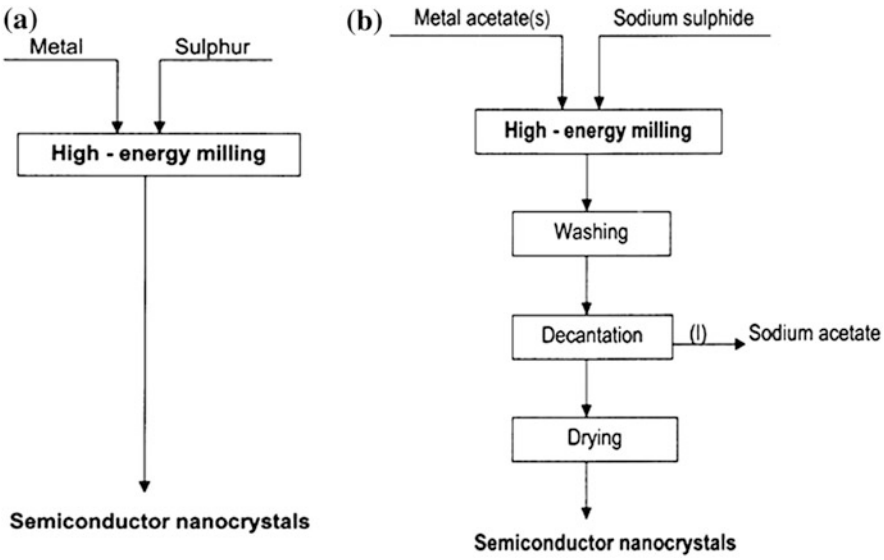


**Fig. 6** Mechanochemical synthesis of sulfides using: (**a**) elemental precursors, (**b**) compounds (metal acetate and sodium sulfide). (Reprinted by permission from Springer Nature Customer Service Centre GmbH: Springer Nature [8] [COPYRIGHT] (2017))

in Fig. 7. The patterns were recorded after 60–180 min of milling. After the first 60 min, only small amounts of desired sulfide are visible next to the non-reacted cobalt and sulfur precursors. Another 60 min of milling was needed to obtain final product cobalt pentlandite $Co_9S_8$ (01-073-6395), which crystallized in the cubic face-centered structure. Further treatment until 180 min did not lead to any significant change in the phase composition.

The transition from paramagnetic to weak ferromagnetic or ferrimagnetic behavior by changing the magnetic field was proven by magnetic measurements (Fig. 8).

## *3.2 Copper Sulfides-Chalcocite $Cu_2S$ and Covellite CuS*

Copper sulfide is a semiconductor with multidisciplinary applications, the ones in biomedicine being of particular interest. In our older studies, we have shown the possibility to prepare this chalcogenide within a second range [13] and that despite the precursors are consumed, the phase transformations still go on for a couple of minutes [14]. The equilibrium was reached after 15 min and 30 min in the case of CuS and $Cu_2S$, respectively. The obtained products were properly characterized using a rich pallette of experimental techniques (SEM/EDS, FTIR, XPS, photoluminescence, nitrogen adsorption, thermal analysis) [15]. In addition, the optical properties by UV-vis spectroscopy were determined (Fig. 9). The optical bandgap of CuS (blue) and $Cu_2S$ was calculated to be 1.92 eV and 3 eV, respectively. In the former case, a red shift in comparison with its bulk analogue was evidenced.

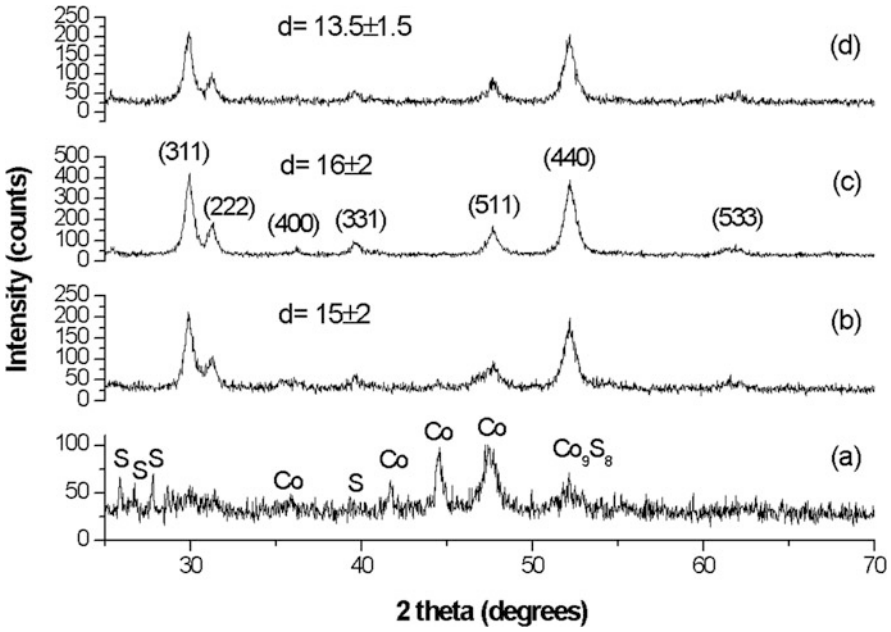


**Fig. 7** XRD patterns of mechanochemically synthesized pentlandite $Co_9S_8$ after different milling time: (**a**) 60 min, (**b**) 90 min, (**c**) 120 min, and (**d**) 180 min. (Reprinted from [12], Copyright (2018), with permission from Elsevier)

The ability of both CuS and $Cu_2S$ to photocatalytically degrade the methyl orange (MO) dye was tested, showing both materials being good photocatalysts. Better results were achieved using $Cu_2S$ (Fig. 9b), as complete degradation of MO dye was observed within 150 min. Covellite (CuS) showed 80% MO degradation after the same duration. Interestingly, the results for the products were better than for the commercial $TiO_2$ (P25) or ZnO. It has to be noted that the adsorption stage was not considered in the experiments and all the decrease in the dye concentration was ascribed to the photocatalytic effect [15].

Mechanochemical synthesis of copper sulfide was also the main topic of the report [16], which was a common work with our Kazakh colleagues. The initial idea was to obtain copper sulfide/sulfur composite by combining the already explained acetate route (milling copper acetate and sodium sulfide) and simultaneously synthesize elemental sulfur (by using sodium thiosulphate as its source and citric acid as a catalyst). However, instead of obtaining CuS/S composite, the needle-like nanocrystals of CuS were obtained. This is of particular interest to mechanochemists, as the shape control is a large issue due to a constant supply of energy and stress to the milled solids, which hampers them from creating a well-crystallized structures. Simultaneously, the problem with synthesis of CuS using acetate route with the formation of oxidized products reported in the past, was also overcome by the proposed methodology. The whole paper is based on the comparison between CuS obtained using the traditional acetate route and the sample prepared by using also the additional sulfur source. The as-received CuS

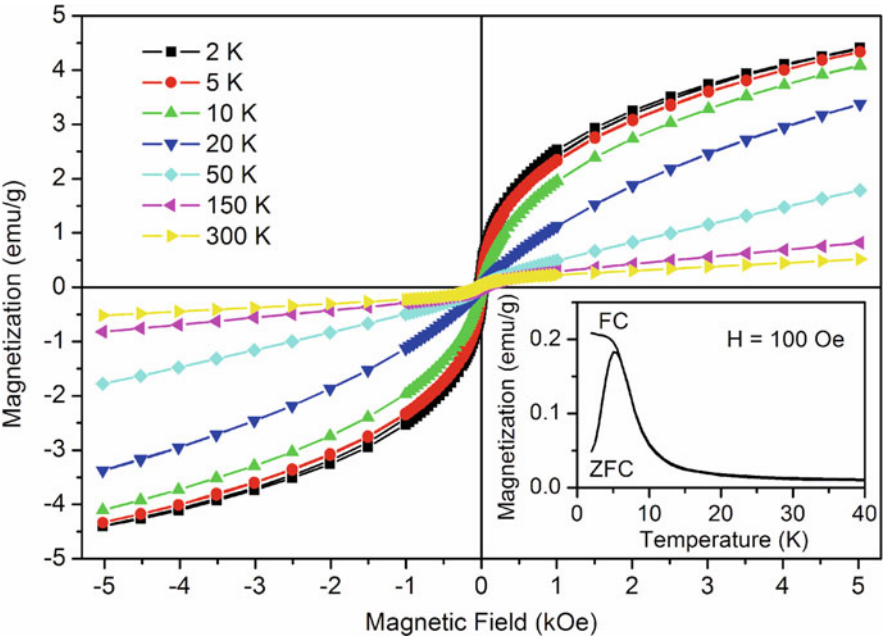


**Fig. 8** Hysteresis loops measured at various temperatures and temperature dependence of magnetization (inset) of mechanochemically synthesized pentlandite $Co_9S_8$ after 120 min of milling. (Reprinted from [12], Copyright (2018), with permission from Elsevier)

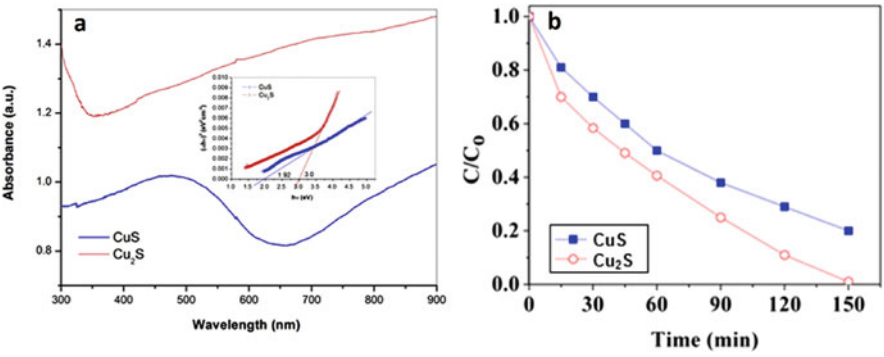


**Fig. 9** (**a**) UV-vis absorption spectra (inset Tauc's plots) of CuS and $Cu_2S$ products. (**b**) The irradiation time-dependent degradation efficiencies of MO solution in the presence of CuS and $Cu_2S$ photocatalysts. (Reprinted from [15], Copyright (2018), with permission from Elsevier)

had a needle-like shape with a uniform thickness of around 6 nm length of up to 60 nm (aspect ratio 1:10), whereas the sample obtained using just copper acetate and sodium sulfide exhibited an isometric morphology with particle size around 20 nm. The formation of the specific morphology in the first case is most probably a result of the presence of elemental sulfur, which may in situ react with CuS by enhancing the $S - S$ bonding and thus causing a preferential growth of CuS along

the basal planes. There was also a significant difference in the grain size (as very often when using the mechanochemical synthesis), the individual nanoparticles are assembled into larger grains, being significantly finer in the case of needle-like CuS, namely, the average grain size was around 340 nm for CuS prepared without using the additional sulfur source and 170 nm when using it. The obtained products were tested as antibacterial agents using the agar well diffusion method, and it was shown that the elongated CuS exhibited activity against both gram-negative *E. coli* and gram-positive *S. aureus*, whereas the other sample was active just against the gram-negative bacteria. The whole story of the paper is summarized in Fig. 10 below.

The mechanochemical synthesis of CuS was also the topic of the study [17]; however, the selected reaction was used just as a model to investigate the amount of iron wear by means of magnetometry. The CuS product was formed in 15 min (in this case, the reaction was much slower than in [13], because the atomized powder Cu with spherical morphology, neither electrolytically prepared Cu powder with needle-like one was used). The possibility to use the magnetization value to calculate the actual amount of iron (even if it is present in trace amounts) in powders treated in steel milling jars was proposed. The amount of iron has rapidly increased between 15 and 30 min of milling, when its content was 0.13 and 0.76%,

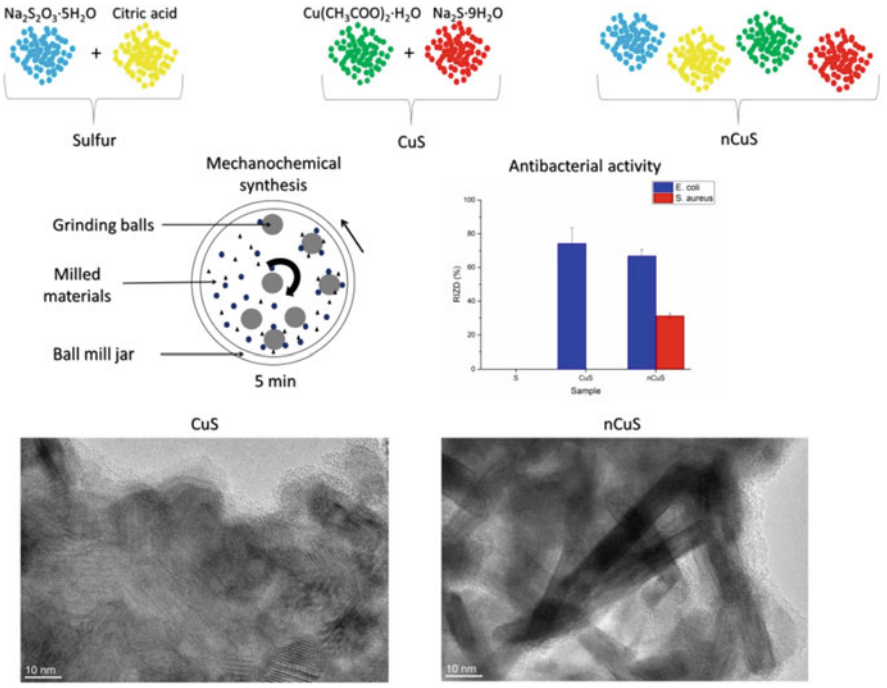


**Fig. 10** Graphical abstract of the report [16] showing the possibility to prepare needle-like CuS nanocrystals using mechanochemical synthesis. (Reprinted with permission from [16]. Copyright 2019 American Chemical Society)

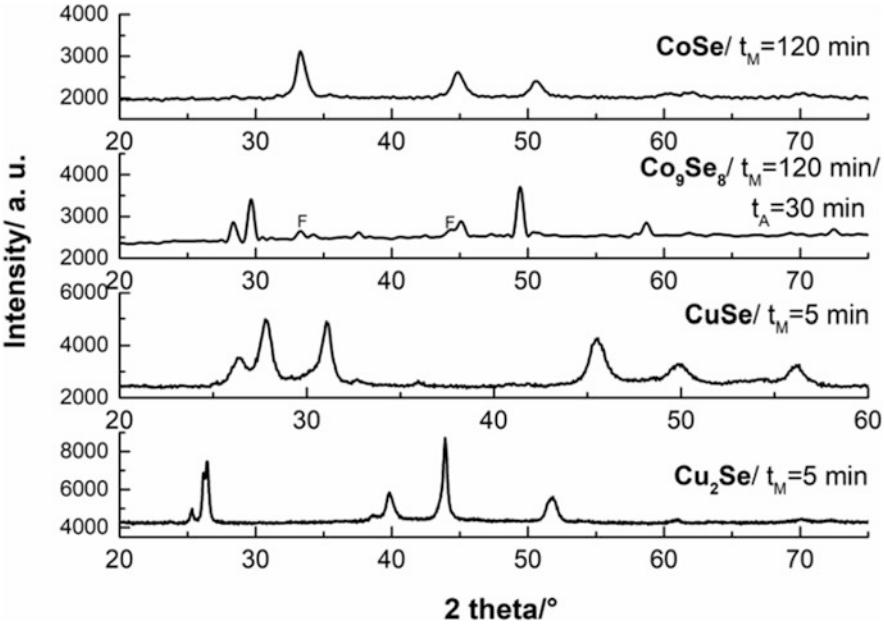


**Fig. 11** X-ray diffraction patterns of synthesized cobalt and copper selenides; $t_M$: milling time, $t_A$: annealing time; F: freboldite-CoSe

respectively. This increase is ascribed to the fact that after 15 min, the reaction is finished and further energy input is used inefficiently.

### *3.3 Co, Cu-Transition-Metal Selenides*

In our recent works, nanostructured CoSe, CuSe, and $Cu_2Se$ semiconductors were successfully synthesized by simple, direct, and relatively inexpensive short-time solid-phase mechanochemical reactions in a high-energy planetary ball mill [18–20]. The synthetic $Co_9Se_8$ with the pentlandite structure, $(Fe,Ni)_9S_8$, was also prepared; however, in this case, also a short subsequent thermal annealing was necessary [21]. The X-ray diffraction patterns of the mechanochemically synthesized cobalt and copper selenides with the corresponding time of mechanochemical synthesis and subsequent thermal treatment, respectively, are shown in Fig. 11.

The diffraction peaks were identified based on the ICDD-PDF cards and correspond to CoSe (freboldite 01-077-7572), $Co_9Se_8$ (01-089-4180), CuSe (00-34-0171), and $Cu_2Se$ (00-47-1448). Rietveld analyses confirmed that mechanochemical synthesis of CoSe is completed after 120 min of milling with an average crystallite size of 26 nm, and mechanochemical/thermal synthesis produced $Co_9Se_8$ nanoparticles with an average crystallite size of 67 nm. After 5 min of milling, CuSe and

$Cu_2Se$ nanoparticles with an average crystallite size of 24 and 25 nm, respectively, were obtained.

TEM/HRTEM images of the agglomerated nanoparticles of prepared Co and Cu-containing transition metal selenides are shown in Fig. 12 and Fig. 13. The larger clusters composed of nanoparticles with tens of nanometer in size were observed in both cases. Within the single agglomerate of $Co_9Se_8$, the crystallites are in close contact, separated by distinct grain boundaries, almost like in sintered ceramics (see Fig. 12b)).

By comparing our mechanochemical synthesis results with the literature, only Campos and co-authors managed to prepare CoSe in more than 72 h by milling in a SPEX shaker mill [22], $Co_9Se_8$ has not been mechanochemically synthesized yet. With regard to copper selenides, Ohtani and co-authors were the only researchers who synthesized γ-CuSe by mechanical alloying for 60 min using a high-energy ball mill [23]. In 2017, Bulat with co-workers produced a single-phase material containing the α-$Cu_2Se$ phase after 2 h of milling in a high-energy ball mill [24] and in 2018, Li and co-workers synthesized almost single-phase β-$Cu_{2-x}Se$ after 20 min of milling in a vibratory mill [25].

The overview table showing the precursors, necessary milling time, achieved particle size, and the application of the binary chalcogenides prepared recently by other research groups is shown below in Table 1.

## 4 Ternary Systems

### *4.1 Chalcopyrite, $CuFeS_2$*

One of the most interesting chalcogenides in ternary systems is chalcopyrite $CuFeS_2$. The rapid mechanochemical synthesis of $CuFeS_2$ particles with good magnetic, optical, and electro-optical properties prepared by high-energy milling in a planetary mill from copper, iron, and sulfur precursors was firstly investigated by our research group [54]. The progress of the mechanochemical synthesis was studied by XRD (Fig. 14). Nanocrystalline $CuFeS_2$ with a tetragonal body-centered crystal structure and crystallite size around 38 nm could be prepared within 60 min of milling. No significant change, either in the lattice parameters or in the microstrain, was observed after prolonged milling until 120 min.

This mineral has been considered as a potential thermoelectric material due to the abundance of the constituting elements, as well as its environmental friendliness. Nanophase and defect formation via milling is a possible route to decrease the fairly high thermal conductivity by increasing phonon scattering. In this respect, mechanochemical pretreatment by high-energy milling in $CuFeS_2$ synthesis is an innovative procedure. Recently, a couple of papers to elucidate the thermoelectric properties of mechanochemically treated chalcopyrite have been published [55–57]. The influence of high-energy milling on structure as well as on the semiconducting

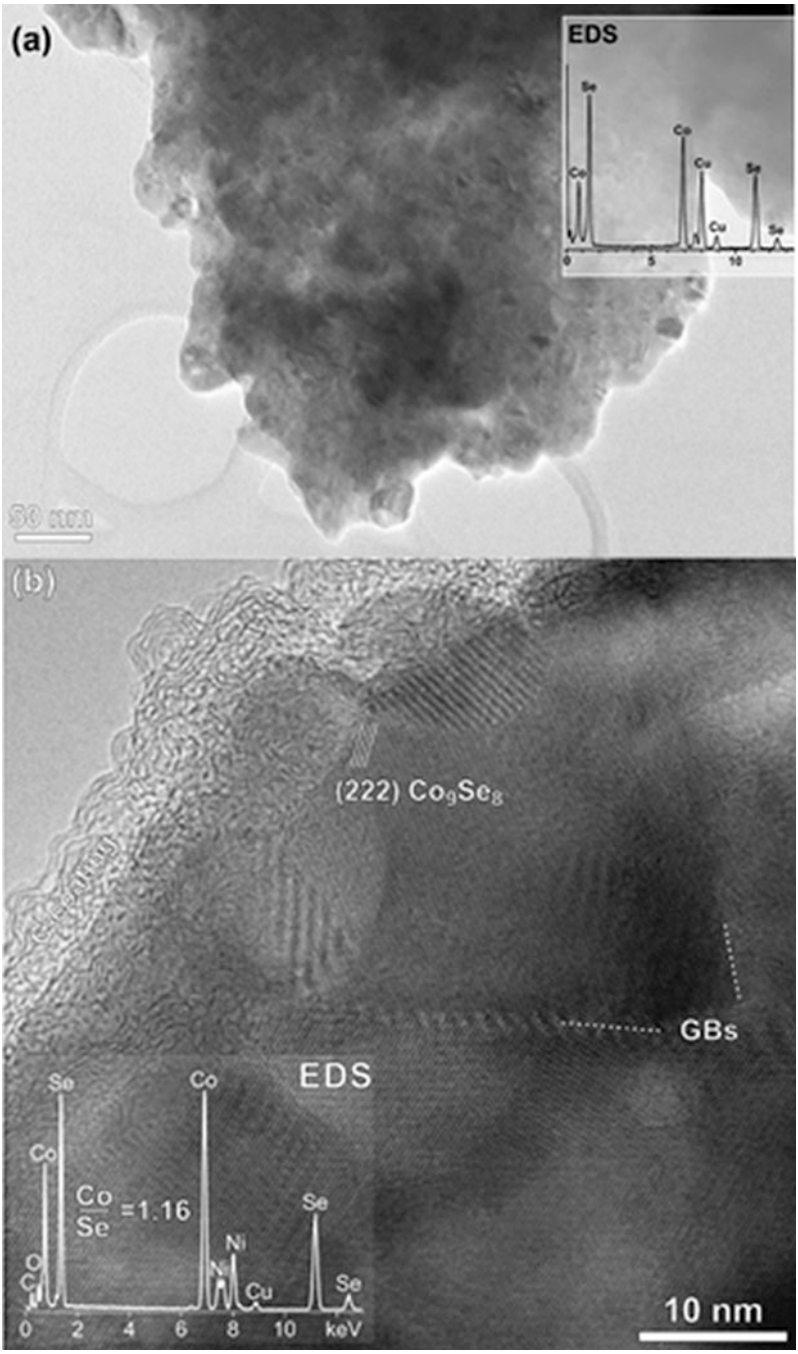


**Fig. 12** (**a**) TEM image of an agglomerated cluster of CoSe nanoparticles with a typical EDS spectrum (inset). The Cu peaks stem from the copper TEM-grid. Reprinted by permission from Springer Nature Customer Service Centre GmbH: Springer Nature [20] [COPYRIGHT] (2017); (**b**) HRTEM image from the thin part of the agglomerate shows larger $Co_9Se_8$ crystallites in close contact (GBs = grain boundaries). EDS analysis from this region yielded Co/Se ratio of 1.16, which is close to 9:8 as expected. Reprinted by permission from Springer Nature Customer Service Centre GmbH: Springer Nature [21] [COPYRIGHT] (2019)

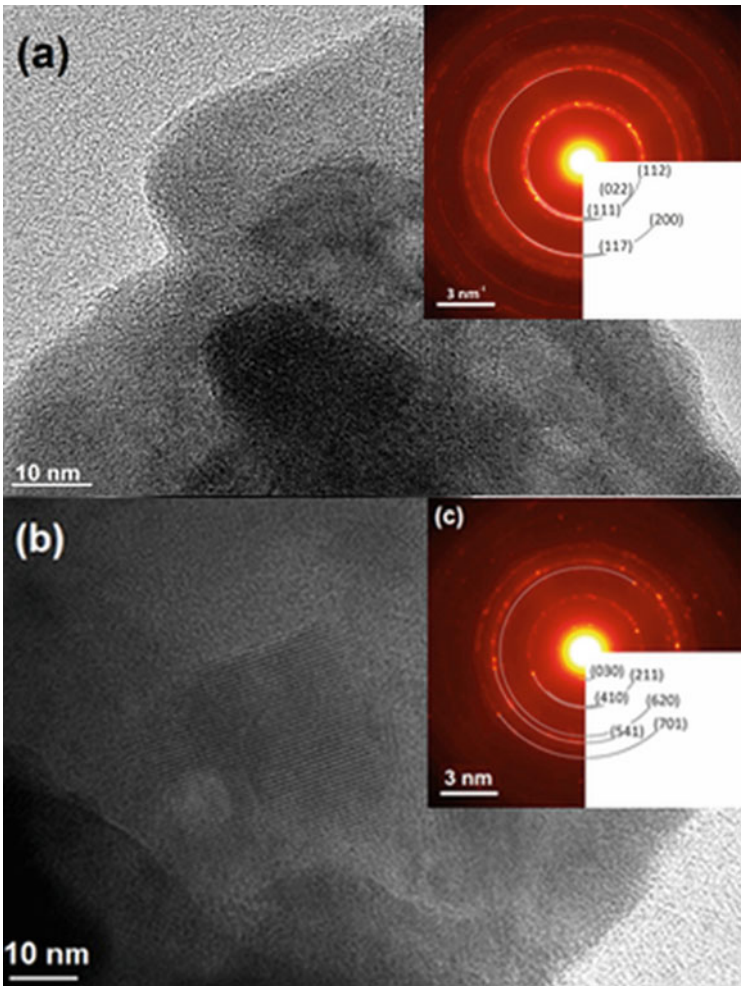


**Fig. 13** (**a**) HRTEM image of agglomerated crystals of CuSe with selected area electron diffraction (SAED) pattern (inset); (**b**) TEM image of agglomerated $Cu_2Se$ crystals; (**c**) SAED pattern of the same crystals. (Reprinted by permission from Springer Nature Customer Service Centre GmbH: Springer Nature [19] [COPYRIGHT] (2021))

properties was studied. While dependence of specific surface area $S_{BET}$ and crystallinity X is already known and tested for several sulfides [10] (Fig. 15 left), a possibility to influence of bandgap is a totally new agenda. In Fig. 15 (right), the dependence of bandgap value on milling time is shown, which illustrates a possibility to manipulate with semiconducting properties (bandgap engineering) of chalcopyrite.

The progress of chalcopyrite synthesis from elements can be also investigated via observing the magnetization changes. This has been accomplished in the study [58].

**Table 1** Overview of binary chalcogenides including selected mechanochemical conditions, obtained crystallite size, and application prepared by other research groups since 2018

| Product | Precursors | Milling time | Particle size | Application | References |
|---|---|---|---|---|---|
| *Sulfides* | | | | | |
| CuS | CuO and S | 22 min | – | Recovery treatment | [26] |
| CuSC, CuS-S-C, CuS-S | C (activated), S, and CuS | 13 h | 10–20 nm | Batteries | [27] |
| $Cu_2S$ | $CuCl_2$, benzene-1,3,5-tricarboxaldehyde and 2,5-diaminobenzene sulfonic acid | 45 min | 40–70 nm | Catalyst | [28] |
| $Fe_{1-X}S$ (x = 0–0.2) | $FeCl_3$ and four different sulfur sources: $Na_2S•9H_2O$, $CH_3CSNH_2$, $Na_2S_2O_3$ and $NH_2CSNH_2$ | 2 h | 10–20 nm | Catalyst | [29] |
| $FeS_x$ (x = 1, 2) | Fe, S, $Li_2S·P_2S_5$ | 10 h and 30 h | 1–3 μm | Batteries | [30] |
| $FeS_{1.92}$ | Mackinawite (FeS) and S | 3 h | Micron scale | Organic waste remediation and catalyst | [31] |
| $Fe_9S_8$ | Fe and S | 2 h | 9–15 nm | Catalyst | [32] |
| $Ga_2S_3$ | Ga and S | 4 h | 42–420 nm | – | [33] |
| $MoS_3$ | $MoS_2$ and S | 10 h | Micron scale | Batteries | [34] |
| $NiS_{1.03}$, $NiS_2$ and $Ni_3S_2$ | Ni and S | 1–8 h | 10–20 nm | – | [35] |
| $Ni_9S_8$ | Ni and S | 2 h | 9–15 nm | Catalyst | [32] |
| NiS-C | $NiCl_2$ and $NH_2CSNH_2$ | 3 h | 20–50 nm | Catalyst | [36] |
| PbS | PbO and $Na_2S$ | 1 h | 11–24 nm | – | [37] |
| RuS-C | $RuCl_3$ and $NH_2CSNH_2$ | 3 h | 20–50 nm | Catalyst | [36] |
| SnS | $C_6H_{15}NO_3$, $SnCl_2·2H_2O$, $C_2H_5NS$ and $NH_3$ | 1–3 h | 20–100 nm | – | [38] |

(continued)

**Table 1** (continued)

| Product | Precursors | Milling time | Particle size | Application | References |
|---|---|---|---|---|---|
| | Sn and S | 2 h | 10–13 nm | Batteries | [39] |
| | Sn and S | 5 h | 15 nm | Solar cells | [40] |
| ZnS | Zn and S | 30 to 45 min | – | – | [41] |
| | Zn, S, and Mn | 90 min | 5–20 nm | – | [42] |
| | $Zn(OAc)_2 \cdot 2H_2O$, $Na_2S \cdot 9H_2O$ and sodium dodecyl benzene sulfonate | 40 min | 1–8 nm | – | [43] |
| | Zn and S | 14–16 h | 200 nm | – | [44] |
| | $ZnCl_2$, $AcCl_3$ and $Na_2S$ | 16 h | 4–18 nm | Diodes | [45] |
| *Selenides* | | | | | |
| CdSe | Cadmium acetate, $FeCl_3.6H_2O$ and $Na_2O_3Se$ | 35 min | 100–150 nm | – | [46] |
| $Cu_{2-x}Se$ ($0.03 \leq x \leq 0.23$) | Cu and Se | 2 h | – | – | [47] |
| $Cu_{2-x}Se$ | Cu and Se | 5–60 min | – | | [25] |
| $Sb_2Se_3$ | Sb and Se | 12 h | 5–15 nm | Batteries | [48] |
| *Tellurides* | | | | | |
| NiTe, $NiTe_2$ and $Ni_2Te_3$ | Ni and Te | 1–12 h | 10–20 nm | – | [49] |
| $Ni_3Te_2$ | Ni and Te | 3–20 h | 4–10 nm | Sensors | [50] |
| $P_{0.8}Te_{0.2}$ | P (red) and Te | 0–80 h | – | – | [51] |
| $Pr_{3-x}Te_4$ ($x = 0 - 0.33$) | Pr and Te (shot) | 10 h | 43–61 nm | Thermoelectrics | [52] |
| $Sc_2Te_3$ | Sc and Te (shot) | 10 h | Micron scale | Thermoelectrics | [53] |

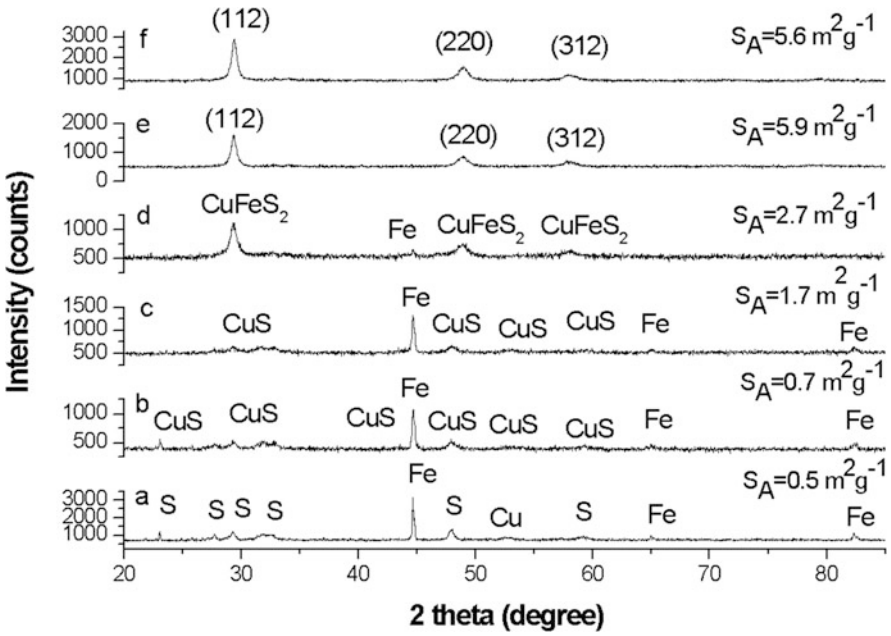


**Fig. 14** XRD patterns of Cu-Fe-S powders before milling (**a**) and after 5 min (**b**), 15 min (**c**), 30 min (**d**), 60 min (**e**), and 120 min (**f**) of milling (the lines labelled by their Miller indexes alone belong to $CuFeS_2$ nanoparticles). (Reprinted with permission from Ref. [54]. Copyright 2018, Elsevier)

Namely, at the beginning, the magnetism is very high due to the presence of highly magnetic elemental iron. As it becomes incorporated into chalcopyrite structure, the magnetization value decreases rapidly (from around 65 $Am^2/kg$ to around 2 $Am^2/kg$ upon 120 min of milling).

## *4.2 Copper Antimony Sulfides-:Chalcostibite, $CuSbS_2$ and Famatinite, $Cu_3SbS_4$*

$CuSbS_2$ nanocrystals were mechanochemically prepared in an argon atmosphere after only 30 min of milling in a laboratory planetary mill [59]. The progress of mechanochemical synthesis is illustrated in Fig. 16 by means of XRD. The analysis validated the formation of orthorhombic structure of $CuSbS_2$ with crystallite size around 25 nm determined by LeBail refinement. UV-vis spectrum revealed absorption of $CuSbS_2$ nanocrystals in the entire visible range with the determined optical bandgap 1.54 eV.

The formation of nanocrystalline chalcostibite $CuSbS_2$ was also validated by transmission electron microscopy (Fig. 17). The sample consists of small nanocrys-

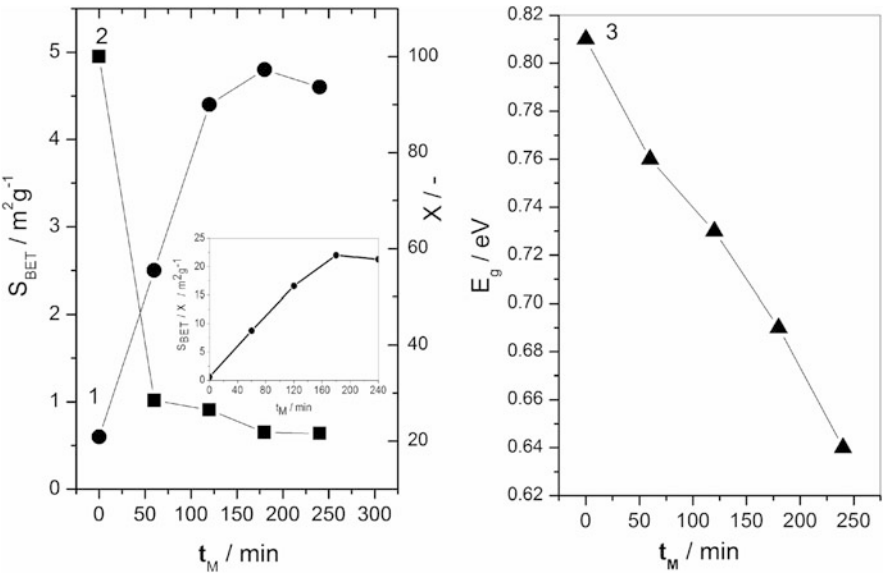


**Fig. 15** The influence of milling time, $t_M$ on specific surface area, $S_{BET}$ (1), crystallinity, X (2) and bandgap, $E_g$ (3) for chalcopyrite $CuFeS_2$. (Reprinted with permission from Ref. [57]. Copyright 2018, Elsevier)

talline domains, which aggregate giving rise to larger particles as can be observed in the TEM image (Fig. 17a). All the SAED rings (Fig. 17a (inset) could be indexed in the orthorhombic symmetry of the $CuSbS_2$, thus being in accordance with the XRD results (Fig. 16). HRTEM images (Fig. 17c, d) indicate nanocrystals directed along two distinct zone axes.

In addition to chalcostibite, $CuSbS_2$, also famatinite $Cu_3SbS_4$ was mechanochemically synthesized using copper, antimony, and sulfur in a stoichiometric ratio 3:1:4 in a planetary ball mill with the utilization of protective atmosphere without the next post-heating [60]. The progress of the mechanochemical synthesis of $Cu_3SbS_4$ for milling times 60–120 min is illustrated in Fig. 18.

The mechanochemical reaction was completed after 120 min of milling, when no other phases could be detected in the XRD pattern, indicating the high purity of the product. The crystallite size 14 nm of the prepared tetragonal famatinite was calculated by LeBail refinement.

The optical properties of $Cu_3SbS_4$ were studied using UV-vis spectroscopy (Fig. 19). The Tauc plot to deduce the direct bandgap from derived UV-vis spectrum is shown as an inset of Fig. 19. The determined direct optical bandgap 1.31 eV is blue-shifted relatively to the bulk $Cu_3SbS_4$. The observed blue shift could be attributed to the existence of very small nanocrystallites.

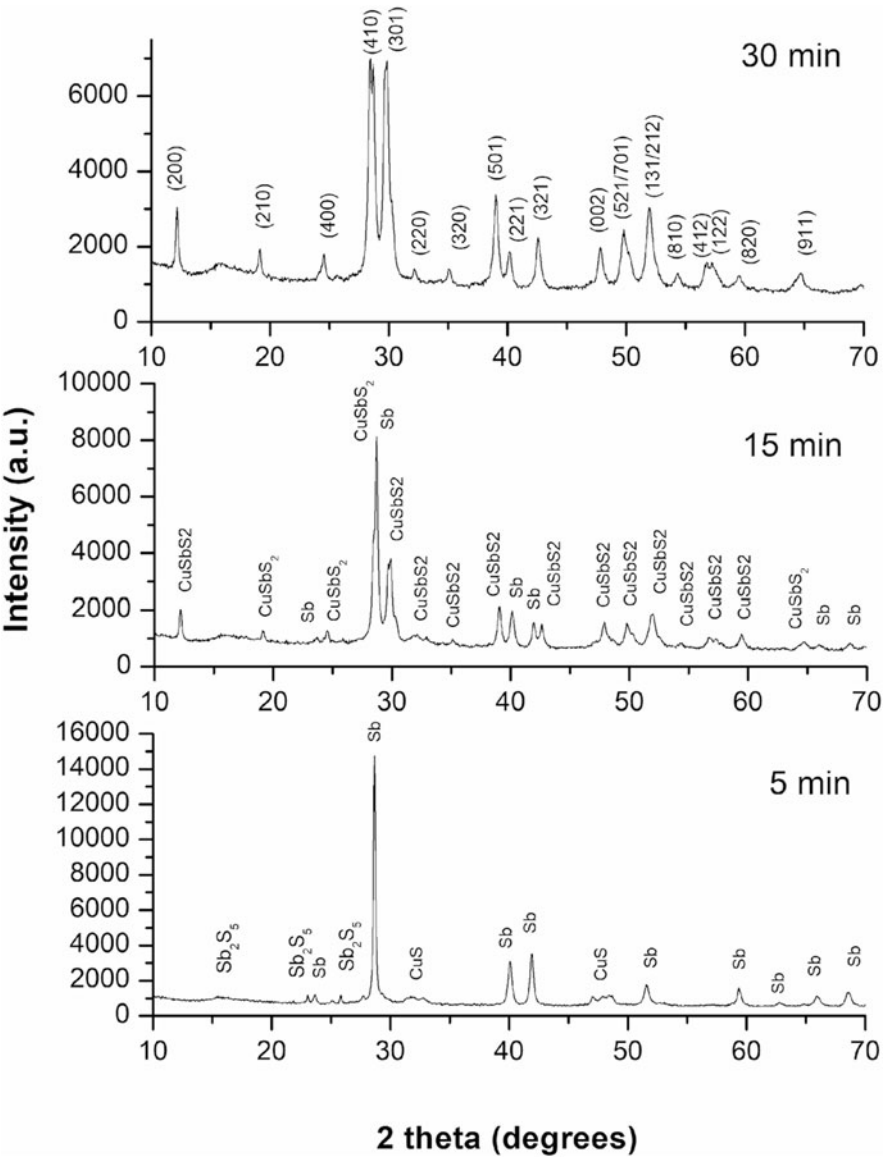


**Fig. 16** XRD patterns of $CuSbS_2$ synthesized for different milling times (the Miller indices in the upper-most pattern belong to $CuSbS_2$ nanoparticles). (Reprinted by permission from Springer Nature Customer Service Centre GmbH: Springer Nature [59] [COPYRIGHT] (2021))

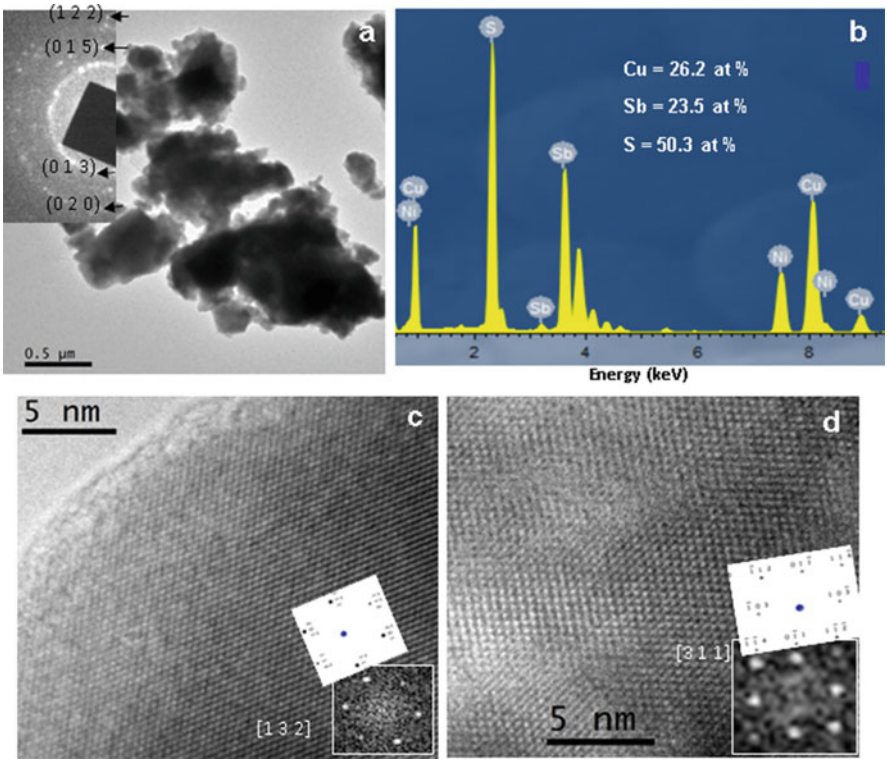


**Fig. 17** TEM analysis of mechanochemically synthesized $CuSbS_2$: TEM image at low magnification with indexed SAED pattern (inset) (**a**), EDS spectrum (**b**), HRTEM images and the corresponding FFTs and simulated ED patterns (inset) (**c**, **d**). (Reprinted by permission from Springer Nature Customer Service Centre GmbH: Springer Nature [59] [COPYRIGHT] (2021))

## *4.3 Copper Tin Sulfide Mohite, $Cu_2SnS_3$*

By means of mechanochemical synthesis, we managed to prepare $Cu_2SnS_3$ (mohite) phase in 15 min using planetary ball milling starting from elements [61]. The XRD patterns measured after 15 s, 5, 10, 15, and 30 min are shown in Fig. 20a. Already after a few seconds, the elemental Cu and S rapidly reacted to form CuS (already after 15 s, the diffractions of CuS are visible). The exothermic reaction of CuS formation is in line with the phenomena described in [13] and was corroborated by a significant increase of pressure in the milling chamber after about 13 s. Until 15 min, tin, together with additional sulfur, was subsequently incorporated into the crystal structure. Further milling did not bring about any changes in the phase composition, only the occurrence of agglomeration phenomenon. The product was in the form of nanocrystals embedded in large micron-sized agglomerates. The presence of small nanocrystals was confirmed by TEM (HRTEM), showing that the size of all the

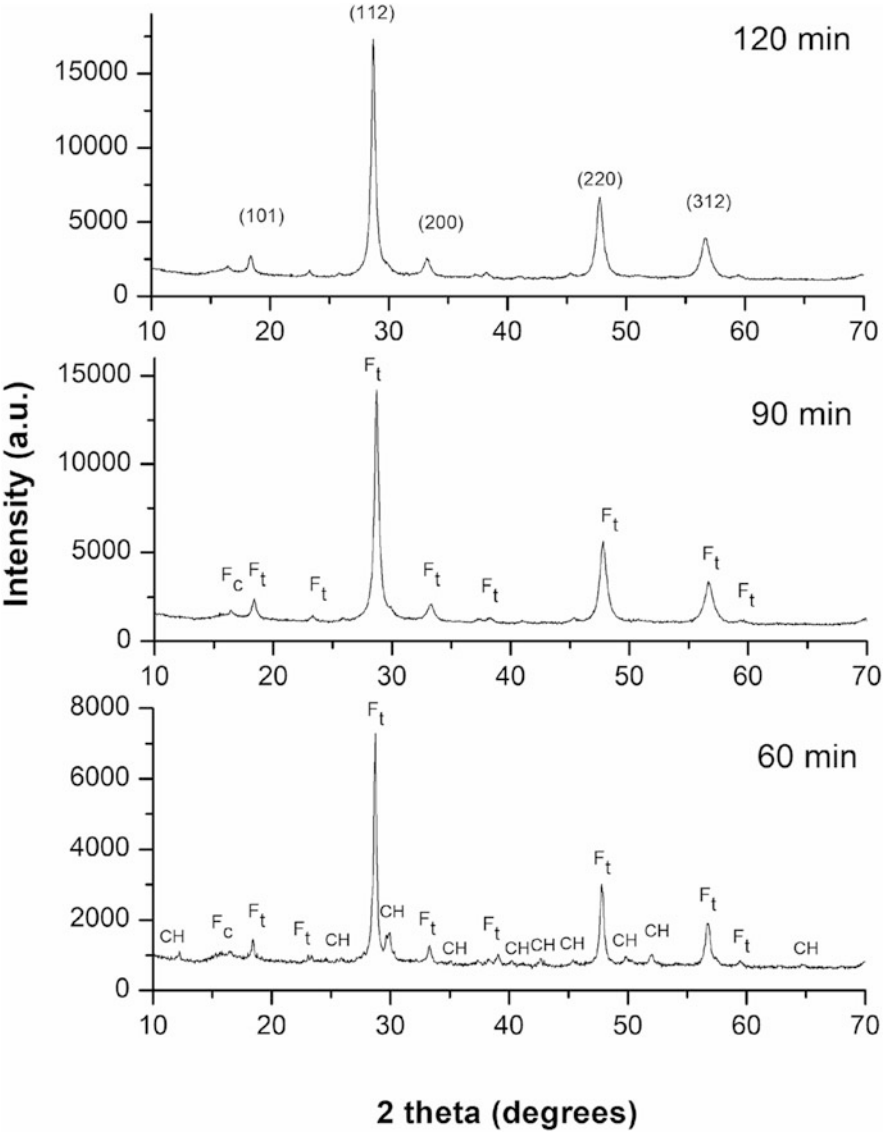


**Fig. 18** XRD patterns of $Cu_3SbS_4$ synthesized in laboratory mill for different milling time. The identified phases are marked as follows: $CuSbS_2$ – chalcostibite (CH), $Cu_3SbS_4$ – tetragonal famatinite ($F_t$), $Cu_3SbS_4$ – cubic famatinite ($F_c$). (Reprinted with permission from Ref. [60]. Copyright 2021, Elsevier)

nanocrystals was below 20 nm (Fig. 20b). The obtained crystals were defective, and such planar defects are marked by an arrow in the figure. The electrical resistivity showing a clear negative correlation with the grain size was also discovered therein.

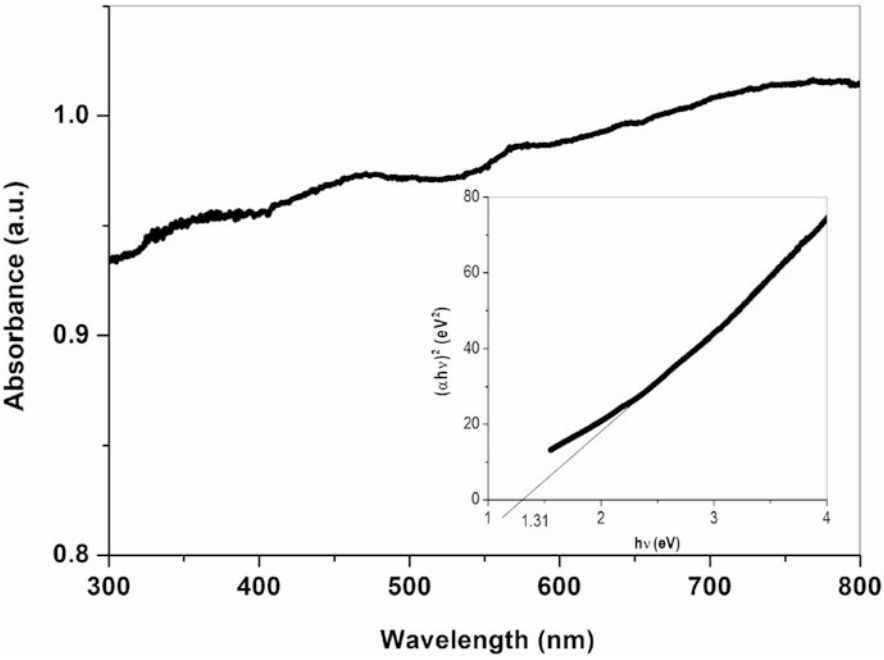


**Fig. 19** UV-vis spectrum of mechanochemically synthesized $Cu_3SbS_4$ and Tauc plot (inset). (Reprinted with permission from Ref. [60]. Copyright 2021, Elsevier)

Very recently, an update to this study concentrating mainly on the Raman spectroscopy characterization of these samples was published. Due to the high sensitivity of Raman spectroscopy, an additional phase of copper sulfate was found, and its presence was postively correlated with the amount of CuS phase, which most probably serves as a precursor of its formation. Thus, the sample after 15 min was the most stable [62].

In our research, we also managed to obtain pure $Cu_2SnS_3$ phase after 60 min of milling in a laboratory planetary ball mill using covellite CuS and SnS (previously obtained by a mechanochemical synthesis) as precursors. The obtained nanocrystals exhibited size of approximately 10–15 nm. Reaction progress calculated from the Rietveld refinement of the XRD patterns is illustrated in Fig. 21a, where the dependence of conversion degree on milling time is shown. Since CTS phase exists in several polymorphs not detectable by XRD, the Raman spectroscopy was used for deeper inspection (Fig. 21b). There was a peak broadening due to the phonon confinement effect. The peak with a maximum at 335 $cm^{-1}$ is undoubtedly assigned to the tetragonal CTS phase. The Raman spectroscopy revealed also the presence of impurities like CuS, SnS, and $SnS_2$, which are formed as intermediates during the mechanochemical synthesis.

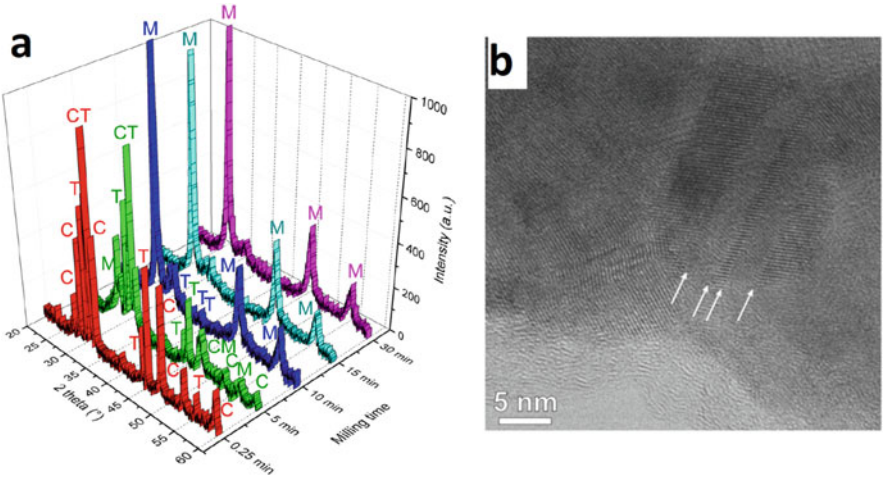


**Fig. 20** (**a**) XRD patterns of the copper-tin-sulfur reaction mixtures milled for different time. The identified crystallographic phases are marked in the figure as follows: C—covellite (JCPDS 00–006-0464), T—tin (JCPDS 03–065-0296), M—mohite (JCPDS00–027-0198), (**b**) HRTEM image showing the $Cu_2SnS_3$ product obtained after 15 min of milling of the stoichiometric elemental mixture. The arrows point to the planar defects. (Reprinted by permission from Springer Nature Customer Service Centre GmbH: Springer Nature [61] [COPYRIGHT] (2018))

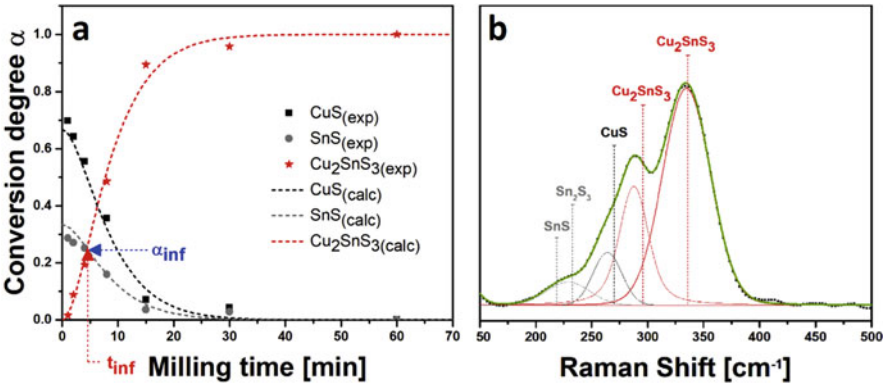


**Fig. 21** (**a**) Reaction kinetics of $Cu_2SnS_3$ synthesis in a laboratory mill calculated from the XRD data using the Rietveld refinement, (**b**) fitted Raman spectra of the product synthesized after 60 min. (Reprinted with permission from Ref. [63]. Copyright 2018, Elsevier)

The overview table showing the precursors, necessary milling time, achieved particle size, and the application of the ternary chalcogenides prepared recently by other research groups is shown below (Table 2).

**Table 2** Overview of ternary chalcogenides prepared by other research groups since 2018

| Product | Precursors | Milling time | Particle size | Application | References |
|---|---|---|---|---|---|
| *Sulfides* | | | | | |
| $AgInS_2$ | S, AgI, $In(ac)_3$, oleyl amine and 1-DDT (1-dodecanethiol) | 2–4 min | 2–5 nm | – | [64] |
| $CuInS_2$ | S, CuBr, $In(ac)_3$, oleyl amine and 1-DDT (1-dodecanethiol) | 2–4 min | 2–5 nm | – | [64] |
| | $Cu_2S$ and $In_2S_3$ | 1 h | 9 nm | – | [65] |
| $Cu_3SbS_4$<br>$Cu_3SbS_3$ | Cu, Sb and S | 2 h | Micron scale | – | [66] |
| $Cu_{12}Sb_4S_{13}$ | $Cu_2S$, CuS, $Sb_2S_3$ | 30 min to 6 h | – | Thermoelectrics | [67] |
| | Cu, Sb, and S | 2 h | Micron scale | – | [66] |
| $Fe_xNi_{9-X}S_8$<br>(x = 0–9) | Fe, Ni, and S | 2 h | 9–15 nm | Catalyst | [32] |
| $Fe_{4.5}Ni_{4.5}S_8$ | Fe, Ni, and S | 15–60 min | 250 nm | Catalyst | [68] |
| $Li_4P_2S_6$ and $xLi_2S.(100-x)P_2S_5$<br>(x = 50, 75 and 80) | S, P (red), $Li_2S$, and $P_2S_5$ | 10 h | – | Batteries | [69] |
| $Li_2S$-$P_2S_5$ and<br>$Li_2S$-$SiS_2$ | $Li_2S$, $P_2S_5$ or $SiS_2$ | 20 min – 20 h | 5 nm | Batteries | [70] |
| $Li_3SbS_4$ | $Li_2S$, $Sb_2S_3$ and S | 100 h | Micron scale | Thermoelectrics | [71] |
| $Li_4SnS_4$<br>$Li_3PS_4$ | $Li_2S$, $SnS_2$, $P_2S_5$ and LiI | 10–60 h | – | Batteries | [72] |
| $Na_2TiS_3$ | $Na_2S$ and $TiS_2$ | 10 h | – | Batteries | [73] |
| PbS/Ni–Cr | Ni–Cr and PbS | 3 h | 15–25 nm | – | [74] |
| Ru-Ni-S | $NiCl_2$, $RuCl_3$ and $NH_2CSNH_2$ | 2 h | 20–50 nm | Catalyst | [36] |
| *Selenides* | | | | | |
| $AgInSe_2$ | Se, AgI, $In(ac)_3$, oleyl amine and 1-DDT (1-dodecanethiol) | 2–4 min | 2–5 nm | – | [64] |
| $CuInSe_2$ | Se, CuBr, $In(ac)_3$, oleyl amine and 1-DDT (1-dodecanethiol) | 2–4 min | 2–5 nm | – | [64] |

## 5 Quaternary Systems

From the quaternary systems, most of our work was devoted to Cu-Fe-Sn-S and Cu-Zn-Sn-S systems. Initially, we planned to apply the obtained materials as adsorber layer in the solar cells; however, the manufacturing of actual cell was necessary to test the performance, and this was not feasible, so therefore, we turned to testing these compounds as potential thermoelectric materials.

### *5.1 Stannite, $Cu_2FeSnS_4$*

With regard to Cu-Fe-Sn-S (CFTS) system, we have intensively investigated the mechanochemical synthesis of stannite $Cu_2FeSnS_4$ phase in the past [75–77]. The synthesis included a rapid formation of CuS as the first step, then incorporation of tin and finally iron into the structure. However, there was always an admixture of rhodostannite $Cu_2FeSn_3S_8$ phase. More recently, two studies describing the spectroscopic properties of the CFTS nanocrystals were published. In the first one [78], the detailed far-infrared study on the prepared CFTS nanocrystals was conducted, and as demonstrated in the spectra obtained for the sample milled for different times, the signals corresponding to binary sulfides (reaction intermediates) disappear with time to reach only CFTS after 2 h of the treatment (Fig. 22). The same facts have been confirmed in another study utilizing Raman measurements [79].

### *5.2 Kesterite, $Cu_2ZnSnS_4$*

We also succeeded in mechanochemically synthesizing the analogue with zinc (instead of iron), which is called kesterite, $Cu_2ZnSnS_4$ (CZTS) [80]. We have investigated an option to prepare it by using elemental precursors and also a mixture of compounds and elements (see equations below):

$$2\,\mathrm{Cu} + \mathrm{Zn} + \mathrm{Sn} + 4\,\mathrm{S} \rightarrow \mathrm{Cu_2ZnSnS_4} \tag{1}$$

$$2\,\mathrm{CuS} + \mathrm{SnS} + \mathrm{Zn} + \mathrm{S} \rightarrow \mathrm{Cu_2ZnSnS_4} \tag{2}$$

The reaction pathway is of course different depending on the option selected. Whereas when the combination of compounds and elements is used, CuS and SnS react to form $Cu_2SnS_3$, and the elements react to form ZnS (Fig. 23, left), the immediate formation of CuS and subsequent incorporation of Sn and Zn takes place in the other case (Fig. 23, right). In both cases, the pure kesterite phase was obtained after 60 min of milling, although in the last 30 min, just the incorporation of last traces of zinc takes place.

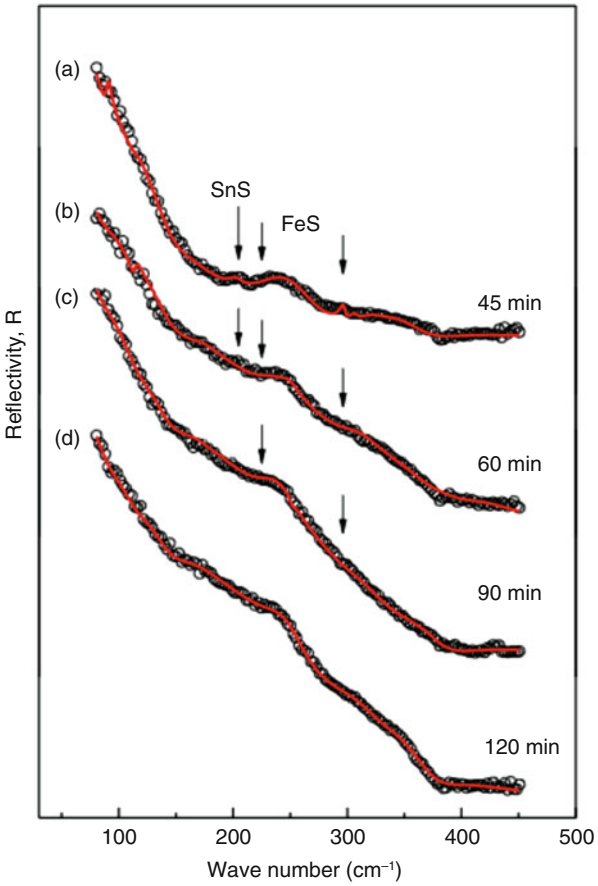


**Fig. 22** Far-infrared reflection spectra of stannite $Cu_2FeSnS_4$ obtained after different milling times (given in the figure). Experimental spectra are presented by circles. The solid lines are calculated spectra obtained by a fitting procedure based on the Maxwell-Garnet mixing rule. (Reprinted with permission from Ref. [78]. Copyright 2018, Elsevier)

TEM analysis has shown that in both cases, the CZTS nanocrystals have the size ranging from 5 to 20 nm and that they contain defects. The elemental distribution seems to be slightly better in the case of the sample prepared by a combination of compounds and elements.

The overview table showing the precursors, necessary milling time, achieved particle size, and the application of quaternary chalcogenides prepared recently by other research groups is shown below (Table 3). Similarly to ternary chalcogenides, only the reports on sulfides were found.

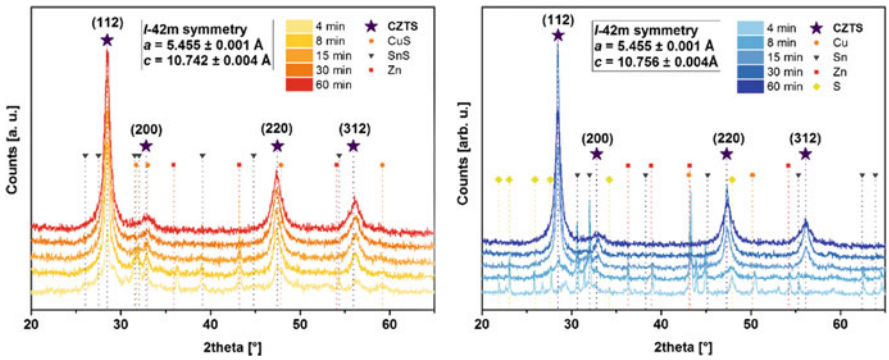


**Fig. 23** X-ray diffraction patterns of stoichiometric mixtures milled according to Eq. 2 (from compounds/elements mixture) (**a**) and Eq. 1 (from elements) (**b**) for various times. (Reprinted with permission from Ref. [80]. Copyright 2019, Elsevier)

## 6 Scale-Up of Mechanochemical Synthesis of Chalcogenides

Although the lab-scale processing opens up new research pathways and leaves enough space for scientists to investigate interesting phenomena, the large-scale production is always questioned by the companies and the applied research. Mechanochemistry is well-scalable; however, only selected methods are suitable for it. In our research, we have shown that the synthesis of chalcogenides can be well-performed in a scalable manner by using eccentric vibratory milling. In this section, we provide a brief overview to show the feasibility of scalable mechanochemical synthesis of chalcogenides via this method.

The concept of eccentric vibratory mill (ESM) has been developed in Germany by the group of professor Gock [92, 93]. The schematic view of the ESM and its photograph is provided in Fig. 24a and b, respectively. The key difference in comparison with the traditional vibratory mills is that this mill produces elliptic, circular, and linear vibrations, which lead to unequalled amplitudes of vibration up to 20 mm and a high degree of disaggregation of the grinding media. This results in more intensive milling, and the specific energy consumption is reduced by 50%.

As it can be seen in Fig. 24b, there is a gray vessel in the middle of the front wall of the mill. This is called a "satellite" chamber and mirrors the exact events going on inside of the big mill (capable of the treatment of tens of kilograms) in a smaller volume. In this configuration, milling of the overall mass up to hundreds of grams is possible, and in our research, we have mostly used this satellite chamber.

The overview table showing various chalcogenides synthesized by our research group using an eccentric vibratory milling (in a satellite chamber) together with the information about the batch size and milling time is provided in Table 4. As

**Table 3** Overview of quaternary chalcogenides prepared by other research groups since 2018

| Product | Precursors | Milling time | Particle size | Application | References |
|---|---|---|---|---|---|
| *Sulfides* | | | | | |
| $Ag_2FeGeS_4$ | $Ag_2S$, $FeS_2$, $GeS_2$, Fe | 4 h | Micron scale | – | [81] |
| $Ag_2MgSn_3S_8$ | MgS, SnS, S, and $Ag_2S$ | 4 h | 4–36 nm | – | [82] |
| $Cu_2MgSn_3S_8$ | MgS, SnS, S, and CuS | 4 h | 4–36 nm | – | [82] |
| $Cu_{1.92}ZnSnS_4$ | Cu, Sn, ZnS, and S | 2 h | 11–13 nm | Solar cells | [83] |
| $Cu_2ZnSnS_4$ | Cu, Zn, Sn, and S | 1–10 h | 12–14 nm | - | [84] |
| | Cu, Zn, Sn, and S<br>or<br>$Cu_2S$, ZnS, SnS, and S | 4 h or 20 h | 10–90 nm or 10–50 nm | – | [85] |
| | Cu, Zn, Sn and S | 5 h | – | Solar cells | [86] |
| $Cu_2ZnGeS_4$ | Cu, Zn, Ge and S | 5 h | – | Solar cells | [86] |
| $Li_2MSn_3S_8$ (M = Mg, Mn, Fe or Ni) | $Li_2S$, SnS, $CoS_2$, S, and $FeS_2$ or MS (M = Mg, Mn, Ni) | 4 h | – | Batteries | [87] |
| $Na_2MgSnS_4$ | SnS, $Na_2S$, MgS, and S | 4 h | Micron scale | – | [88] |
| $Na_{3-x}P_{1-x}W_xS_4$ ($0 \leq x \leq 0.24$) | $Na_2S$, $P_2S_5$, S and $WS_2$ | 15 h | Micron scale | Batteries | [89] |
| $Na_{3+x}Sb_{1-x}M_xS_4$ (M = Si, Ge, Sn; x = 0.03, 0.06, 0.09) | $Na_2S$, $Sb_2S_3$,<br>S and<br>$SiS_2$ or $SnS_2$ $GeS_2$ | 30 h | – | Batteries | [90] |
| $Na_{3-x}Sb_{1-x}Mo_xS_4$<br>(x = 0.06, 0.12, 0.18, 0.24) | $Na_2S$, $Sb_2S_3$,<br>S, and<br>$MoS_2$ | 30 h | – | Batteries | [90] |
| *Selenides* | | | | | |
| $Cu_2ZnMSe_4$ M = Ge, Sn | Cu, Zn, Sn, Ge, and Se | 5 h | – | Solar cells | [86] |
| $Na_{11}Sn_2PSe_{12}$ | Na, Sn, P, and Se | 10–15 h | Micron scale | Batteries | [91] |

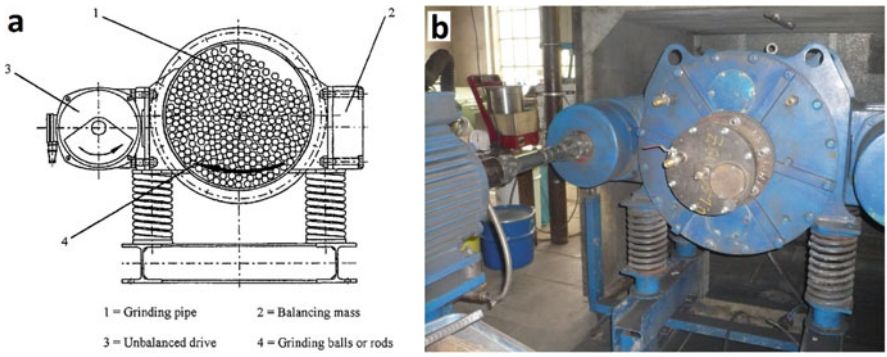


**Fig. 24** Eccentric vibratory mill: (**a**) schematic view, (**b**) photograph. (Part A is reprinted with permission from Ref. [93]. Copyright 1999 Elsevier)

it can be seen, mainly copper-based chalcogenides were synthesized. The duration of milling was usually longer than in the case of lab-scale synthesis; however, the scalability of the process is of utmost importance. Finally, we managed to prepare covellite in 7.5 kg batch upon operating the ESM device in the full mode. In the majority of works, we have evaluated the thermoelectric performance of the prepared chalcogenides.

## 7 Conclusion

In this chapter, mechanochemical synthesis has been shown as a very perspective method to prepare nanocrystalline chalcogenides. The high-energy milling process and the events of mechanical activation and mechanochemical reaction play a decisive role in achieving the products with desired properties. The overview tables have shown that a rich plethora of binary, ternary, and quaternary chalcogenides have been recently prepared by research groups all around the world. The works of our research group focusing on the lab-scale preparation of mainly copper-based sulfides and selenides have been reviewed. The scalability of mechanochemical synthesis upon using eccentric vibratory milling was outlined in the last part of the chapter.

**Table 4** Overview of recent studies of our research group reporting the scalable mechanochemical synthesis using eccentric vibratory mill

| Targeted product | Precursors | Batch | Milling time (min) | Crystallite size | Tested application | References |
|---|---|---|---|---|---|---|
| *Binary* | | | | | | |
| Covellite CuS | Cu, S | 300 g | 40 | 11 nm | | [94] |
| | Cu, S | 7.5 kg | 60 | | | [94] |
| Klockmannite CuSe | Cu, Se | 90.25 g | 10 | 64 nm | – | [18] |
| *Ternary* | | | | | | |
| Mohite $Cu_2SnS_3$ | Cu, Sn, S | 100 g | 180 | | Thermoelectrics | [95] |
| | CuS, SnS | 100 g | 240 | 10–15 nm | | [63] |
| Tetrahedrite $Cu_{12}Sb_4S_{13}$ | Cu, Sb, S | 100 g | 240 | 20 nm | Thermoelectrics | [95] |
| Bi-doped Tetrahedrite $Cu_{12}Sb_4S_{13}$ | Bi, Cu, Sb, S | 100 g | 60 | | Thermoelectrics | [96] |
| Chalcopyrite $CuFeS_2$ | Cu, Fe, S | 100 g | 720 | 10 nm | Thermoelectrics | [95] |
| Famatinite $Cu_3SbS_4$ | Cu, Sb, S | 100 g | 180 | 10 nm | | [60] |
| *Quaternary* | | | | | | |
| Kesterite $Cu_2ZnSnS_4$ | Cu, Zn, Sn, S | 100 g | 240 | | | [97] |
| | Cu, Zn, Sn, S or CuS, SnS, Zn, S | 100 g | 360 | 15 nm | | [80] |
| Stannite $Cu_2FeSnS_4$ | $CuFeS_2$, CuS, SnS | 100 g | 240 | | | [97] |
| | CuS, SnS, Fe, S | 100 g | 480 | | | |
| | Cu, Fe, Sn, S | 100 g | 240 | | | |
| Mawsonite $Cu_6Fe_2SnS_8$ | Cu, Fe, Sn, S | 100 g | 240 | < 1 μm | Thermoelectrics | [98] |
| Rhodostannite $Cu_2FeSn_3S_8$ | Cu, Fe, Sn, S | 100 g | 360 | 12 nm | Thermal insulation | [99] |
| Colusite $Cu_{26}V_2Sn_6S_{32}$ | Cu, V, Sn, S | 100 g | 720 | < 1 μm | Thermoelectrics | [100] |

**Acknowledgments** This work was supported by the projects of the Slovak Research and Development Agency APVV (contract no. 18-0357) and the Scientific Grant Agency of the Ministry of Education, Science, Research and Sport of the Slovak Republic and Slovak Academy of Sciences (2/0112/22, 2/0103/20).

## References

1. G. Heinicke, *Tribochemistry* (Akademie-Verlag, Berlin, 1984), 495 p
2. A.D. McNaught, A. Wilkinson, *IUPAC Compendium of Chemical Terminology ("The Golden Book")*, 2nd edn. (Blackwell Scientific Publication, Oxford, 1997)
3. W. Ostwald, Die chemische Literatur und die Organisation der Wissenschaft, in *Handbuch der Allgemeinen Chemie*, ed. by W. Ostwald, C. Drucker, (Akademische Verlagesellschaft, Leipzig, 1919), pp. 70–77
4. M. Baláž, L. Vella-Zarb, J.G. Hernández, I. Halasz, D.E. Crawford, M. Krupička, et al., Mechanochemistry: A disruptive innovation for the industry of the future. Chim. Oggi **37**, 32–34 (2019)
5. M. Baláž, *Environmental Mechanochemistry: Recycling Waste into Materials Using High-Energy Ball* (Springer, Milling, 2021), 619 p
6. M. Baláž, M. Achimovičová, P. Baláž, E. Dutková, M. Fabián, M. Kováčová, Z. Lukáčová Bujňáková, E. Tóthová, Mechanochemistry as a versatile and scalable tool for nanomaterials synthesis: Recent achievements in Košice, Slovakia. Curr. Opin. Green Sustain. Chem. **24**, 7–13 (2020)
7. P. Baláž, M. Achimovičová, M. Baláž, P. Billik, Z. Cherkezova-Zheleva, J.M. Criado, et al., Hallmarks of mechanochemistry: From nanoparticles to technology. Chem. Soc. Rev. **42**, 7571–7637 (2013)
8. P. Balaz, M. Balaz, M. Achimovicova, Z. Bujinakova, E. Dutkova, Chalcogenide mechanochemistry in materials science: Insight into synthesis and applications (a review). J. Mater. Sci. **52**, 11851–11890 (2017)
9. P. Baláž, *Extractive Metallurgy of Activated Minerals* (Elsevier, Amsterdam, 2000), p. 278
10. P. Baláž, *Mechanochemistry in Nanoscience and Minerals Engineering* (Springer, Berlin/Heidelberg, 2008), p. 413
11. P. Baláž, E. Boldižárová, E. Godočíková, J. Briančin, Mechanochemical route for sulphide nanoparticles preparation. Mater. Lett. **57**, 1585–1589 (2003)
12. E. Dutková, M. Čaplovičová, I. Škorvánek, M. Baláž, A. Zorkovská, P. Baláž, Ľ. Čaplovič, Structural, surface and magnetic properties of chalcogenide $Co_9S_8$ nanoparticles prepared by mechanochemical synthesis. J. Alloys Compd. **745**, 863–867 (2018)
13. M. Baláž, A. Zorkovská, F. Urakaev, P. Baláž, J. Briančin, Z. Bujňáková, M. Achimovičová, E. Gock, Ultrafast mechanochemical synthesis of copper sulfides. RSC Adv. **6**, 87836–87842 (2016)
14. M. Baláž, A. Zorkovská, J.S. Blazquez, N. Daneu, P. Baláž, Mechanochemistry of copper sulphides: Phase interchanges during milling. J. Mater. Sci. **52**, 11947–11961 (2017)
15. M. Baláž, E. Dutková, Z. Bujňáková, E. Tóthová, N.G. Kostova, Y. Karakirova, J. Briančin, M. Kaňuchová, Mechanochemistry of copper sulfides: Characterization, surface oxidation and photocatalytic activity. J. Alloys Compd. **746**, 576–582 (2018)
16. Z. Shalabayev, M. Baláž, N. Daneu, E. Dutková, Z. Bujňáková, M. Kaňuchová, et al., Sulfur-mediated Mechanochemical synthesis of spherical and needle-like copper sulfide nanocrystals with antibacterial activity. ACS Sustain. Chem. Eng. **7**, 12897–12909 (2019)
17. M. Baláž, M. Rajňák, Z. Shalabayev, A. Zubrik, Detection of iron wear in mechanochemistry using magnetometry. Acta Phys. Pol. A **137**, 684–686 (2020)

18. M. Achimovicova, M. Balaz, V. Girman, J. Kurimsky, J. Briancin, E. Dutkova, K. Gaborova, Comparative study of nanostructured CuSe semiconductor synthesized in a planetary and vibratory mill. Nanomaterials **10**, 2038 (2020)
19. K. Gaborova, M. Achimovicova, M. Hegedus, V. Girman, M. Kanuchova, E. Dutkova, Advantageous mechanochemical synthesis of copper(I) selenide semiconductor, characterization, and properties. Front. Chem. Sci. Eng. **16**, 433 (2021)
20. M. Achimovičová, N. Daneu, E. Dutková, A. Zorkovská, Mechanochemically synthesized cobalt monoselenide: Structural characterization and optical properties. Appl. Phys. A Mater. Sci. Process. **123**, 154 (2017)
21. M. Achimovicova, N. Daneu, E. Tothova, M. Mazaj, E. Dutkova, Combined mechanochemical/thermal annealing approach for the synthesis of $Co_9Se_8$ with potential optical properties. Appl. Phys. A Mater. Sci. Process. **125**, 8 (2019)
22. C. Campos, J. de Lima, T. Grandi, K. Machado, P. Pizani, Structural studies of cobalt selenides prepared by mechanical alloying. Phys. B Condens. Matter **324**, 409–418 (2002)
23. T. Ohtani, M. Motoki, K. Koh, K. Ohshima, Synthesis of binary copper chalcogenides by mechanical alloying. Mater. Res. Bull. **30**, 1495–1504 (1995)
24. L. Bulat, V. Osvenskii, A. Ivanov, A. Sorokin, D. Pshenay-Severin, V. Bublik, N. Tabachkova, V. Panchenko, M. Lavrentev, Experimental and theoretical study of the thermoelectric properties of copper selenide. Semiconductors **51**, 854–857 (2017)
25. J. Li, G. Liu, X. Wu, G. He, Z. Yang, J. Li, Reaction mechanism in mechanochemical synthesis of $Cu_2$-xSe. Ceram. Int. **44**, 22172–22175 (2018)
26. M. Masdarian, A. Azizi, Z. Bahri, Mechanochemical sulfidization of a mixed oxide-sulphide copper ore by co-grinding with sulfur and its effect on the flotation efficiency. Chin. J. Chem. Eng. **28**, 743–748 (2020)
27. S.M. Hosseini, A. Varzi, S. Ito, Y. Aihara, S. Passerini, High loading CuS-based cathodes for all-solid-state lithium sulfur batteries with enhanced volumetric capacity. Energy Storage Mater. **27**, 61–68 (2020)
28. S. Kumar, M.B. Gawande, I. Medřík, M. Petr, O. Tomanec, V. Kupka, R.S. Varma, R. Zbořil, Mechanochemical synthesis of $Cu_2S$ bonded 2D-sulfonated organic polymers: Continuous production of dimethyl carbonate (DMC) via preheating of reactants. Green Chem. **22**, 5619–5627 (2020)
29. A. Molla, H. Choi, H. Sakong, J.H. Youk, Sulfur-source dependent wet mechanochemical synthesis of pyrrhotite nanoparticles and evaluation of their sonocatalytic dye degradability. Mater. Res. Bull. **145**, 111519 (2022)
30. M. Pan, T. Hakari, A. Sakuda, A. Hayashi, Y. Suginaka, S. Mori, M. Tatsumisago, Electrochemical properties of all-solid-state lithium batteries with amorphous FeSx-based composite positive electrodes prepared via Mechanochemistry. Electrochemistry **86**, 175–178 (2018)
31. C. Guo, D. Yue, S. Wang, X. Qian, Y. Zhao, Mechanochemically sulfured $FeS_{1.92}$ as stable and efficient heterogeneous Fenton catalyst. Chin. Chem. Lett. **31**, 1978–1981 (2020)
32. H.M. Amin, M. Attia, D. Tetzlaff, U.P. Apfel, Tailoring the Electrocatalytic activity of Pentlandite $Fe_xNi_{9-X}S_8$ nanoparticles via variation of the Fe: Ni ratio for enhanced water oxidation. ChemElectroChem **8**, 3863–3874 (2021)
33. K. Denoue, F. Cheviré, C. Calers, L. Verger, D. Le Coq, L. Calvez, Mechanochemical synthesis and structural characterization of gallium sulfide $Ga_2S_3$. J. Solid State Chem. **292**, 121743 (2020)
34. G. Shirota, A. Nasu, M. Deguchi, A. Sakuda, M. Tatsumisago, A. Hayashi, Electrode performance of amorphous $MoS_3$ in all-solid-state sodium secondary batteries. J. Power Sources Adv. **10**, 100061 (2021)
35. M. Kristl, S. Gyergyek, J. Kristl, Nanostructured nickel sulfides with different Stoichiometries prepared by Mechanochemical synthesis. Chalcogenide Lett. **15**, 55–61 (2018)
36. T.L. Jin, X. Liu, H. Wang, X. Wu, Y. Zhang, Mechanochemical-assisted synthesis of ternary Ru-Ni-S pyrite analogue for enhanced hydrogen evolution performance. Carbon **162**, 172–180 (2020)

37. W. Meng, W. Yuan, Z. Wu, X. Wang, W. Xu, L. Wang, et al., Mechanochemical synthesis of lead sulfide (PbS) nanocrystals from lead oxide. Powder Technol. **347**, 130–135 (2019)
38. A. Kothari, K. Dave, Solution-based deposition of SnS nanostructures from mechanochemically prepared precursor bath. Mater. Lett. **236**, 299–302 (2019)
39. M. Dogrusoz, R. Demir-Cakan, Mechanochemical synthesis of SnS anodes for sodium ion batteries. J. Energy Res. **44**, 10809–10820 (2020)
40. B.-I. Park, Y.H. Jang, S.Y. Lee, D.-K. Lee, Mechanochemically synthesized SnS nanocrystals: Impact of nonstoichiometry on phase purity and solar cell performance. ACS Sustain. Chem. Eng. **6**, 3002–3009 (2018)
41. H. Petersen, S. Reichle, S. Leiting, P. Losch, W. Kersten, T. Rathmann, et al., In situ synchrotron X-ray diffraction studies of the Mechanochemical synthesis of ZnS from its elements. Chem. Eur. J. **27**, 12558 (2021)
42. M.A. Avilés, J. Córdoba, M.J. Sayagués, F. Gotor, Synthesis of Mn 2+-doped ZnS by a mechanically induced self-sustaining reaction. J. Mater. Sci. **55**, 1603–1613 (2020)
43. P. Hu, C. Xie, Z. Mao, X. Liang, A Mechanochemical route for ZnS nanocrystals, and batch sorting along size distribution. Nanomaterials **9**, 1325 (2019)
44. H.-Y. Ahn, W.J. Choi, S.Y. Lee, B.-K. Ju, S.-H. Cho, Mechanochemical synthesis of ZnS for fabrication of transparent ceramics. Res. Chem. Intermed. **44**, 4721–4731 (2018)
45. A. Alshahrie, A. Al-Ghamdi, L.M. Bronstein, Synthesis and characterization of $Zn_{1-x}Ac_xS$ ($0 \leq x \leq 0.1$) nanocrystalline quantum dots prepared via soft mechanochemical approach. Ceram. Int. **45**, 20929–20935 (2019)
46. N. Jafaripour, H. Omidvar, S. Saber-Samandari, R. Mohammadi, R. Shokrani Foroushani, B. Kamyab Moghadas, M. Soleimani, B. Noshadi, A. Khandan, Synthesize and characterization of a novel cadmium selenide nanoparticle with iron precursor applicable in hyperthermia of cancer cells. Int. J. Nanosci. Nanotechnol. **17**, 77–90 (2021)
47. A. Ivanov, I. Tarasova, V. Bublik, R.K. Akchurin, I. Shchetinin, N.Y. Tabachkova, D. Pshenay-Severin, V. Osvenskii, Temperature dependence of the lattice parameters of $Cu_{2-x}Se$ ($0.03 \leq x \leq 0.23$) powders fabricated by mechanochemical synthesis. Phys. Solid State **60**, 2295–2299 (2018)
48. J.-H. Choi, M.-H. Lee, H.-Y. Choi, C.-M. Park, S.-M. Lee, J.-H. Choi, Investigation of electrochemical reaction mechanism for antimony selenide nanocomposite for sodium-ion battery electrodes. J. Appl. Electrochem. **49**, 207–216 (2019)
49. M. Kristl, S. Gyergyek, S.D. Škapin, J. Kristl, Solvent-free mechanochemical synthesis and characterization of nickel tellurides with various Stoichiometries: NiTe, $NiTe_2$ and Ni2$Te_3$. Nanomaterials **11**, 1959 (2021)
50. U.K. de Fatima, J.P. Winiarski, C.L. Jost, C.E.M. de Campos, Mechanochemical synthesis of a $Ni_3$-x$Te_2$ nanocrystalline composite and its application for simultaneous electrochemical detection of dopamine and adrenaline. Compos. Part B Eng. **183**, 107649 (2020)
51. K. Itoh, Y. Mizuhara, T. Otomo, Mechanochemical synthesis of binary phosphorus telluride: Short range structure and thermal properties. J. Solid State Chem. **267**, 119–123 (2018)
52. D. Cheikh, B.E. Hogan, T. Vo, P. Von Allmen, K. Lee, D.M. Smiadak, et al., Praseodymium telluride: A high-temperature, high-ZT thermoelectric material. Joule **2**, 698–709 (2018)
53. D. Cheikh, K. Lee, W. Peng, A. Zevalkink, J.-P. Fleurial, S.K. Bux, Thermoelectric properties of scandium sesquitelluride. Materials **12**, 734 (2019)
54. E. Dutkova, Z. Bujnakova, J. Kovac, I. Skorvanek, M.J. Sayagues, A. Zorkovska, J. Kovac, P. Balaz, Mechanochemical synthesis, structural, magnetic, optical and electrooptical properties of $CuFeS_2$ nanoparticles. Adv. Powder Technol. **29**, 1820–1826 (2018)
55. P. Levinsky, J. Hejtmanek, K. Knizek, M. Pashchenko, J. Navratil, P. Masschelein, E. Dutkova, P. Balaz, Nanograined n- and p-type chalcopyrite $CuFeS_2$ prepared by mechanochemical synthesis and sintered by SPS. Acta Phys. Pol. A **137**, 904–907 (2020)
56. P. Balaz, E. Dutkova, P. Levinsky, N. Daneu, L. Kubickova, K. Knizek, et al., Enhanced thermoelectric performance of chalcopyrite nanocomposite via co-milling of synthetic and natural minerals. Mater. Lett. **275**, 128107 (2020)

57. P. Baláž, E. Dutková, M. Baláž, R. Džunda, J. Navrátil, K. Knížek, P. Levinský, J. Hejtmánek, Mechanochemistry for energy materials: Impact of high-energy milling on chemical, electric and thermal transport properties of chalcopyrite $CuFeS_2$ nanoparticles. ChemistryOpen **10**, 806–814 (2021)
58. P. Baláž, M. Baláž, E. Dutková, M. Hegedus, M. Rajňák, K. Knížek, et al., Magnetization as an effective tool for kinetic evaluation in Mechanochemical synthesis of chalcopyrite $CuFeS_2$. Acta Phys. Pol. A **137**, 647–649 (2020)
59. E. Dutkova, M.J. Sayagues, M. Fabian, J. Kovac, J. Kovac, M. Balaz, M. Stahorsky, Mechanochemical synthesis of ternary chalcogenide chalcostibite $CuSbS_2$ and its characterization. J. Mater. Sci. Mater. Electron. **32**, 22898–22909 (2021)
60. E. Dutkova, M. Sayagues, M. Fabian, M. Balaz, M. Achimovicova, Mechanochemically synthesized ternary chalcogenide $Cu_3SbS_4$ powders in a laboratory and an industrial mill. Mater. Lett. **291**, 129566 (2021)
61. M. Baláž, N. Daneu, M. Rajňák, J. Kurimský, M. Hegedűs, E. Dutková, M. Fabián, M. Kaňuchová, P. Baláž, Rapid mechanochemical synthesis of nanostructured mohite $Cu_2SnS_3$ (CTS). J. Mater. Sci. **53**, 13631–13642 (2018)
62. J. Trajic, M. Curcic, M. Casas Luna, M. Romcevic, M. Remesova, M. Baláž, L. Čelko, K. Dvorek, N. Romcevic, Vibrational properties of the mechanochemically synthesized $Cu_2SnS_3$: Raman study. J. Raman Spectrosc. **53**, 977–987 (2022)
63. M. Hegedüs, M. Baláž, M. Tešinský, M.J. Sayagués, P. Šiffalovič, M. Kruľáková, J. Briančin, M. Fabián, Scalable synthesis of potential solar cell absorber $Cu_2SnS_3$ (CTS) from nanoprecursors. J. Alloys Compd. **768**, 1006–10015 (2018)
64. A. Bera, S.S. Pathak, V. Kotha, B.L. Prasad, Lamellar bimetallic thiolates: Synthesis, characterization, and their utilization for the preparation of bimetallic chalcogenide nanocrystals through Mechanochemical grinding. Adv. Mater. Interfaces **8**, 2100898 (2021)
65. D. Delmonte, R. Manfredi, D. Calestani, F. Mezzadri, L. Righi, M. Mazzer, et al., An affordable method to produce $CuInS_2$ 'mechano-targets' for film deposition. Semicond. Sci. Technol. **35**, 045026 (2020)
66. F. Neves, L. Esperto, I. Figueira, J. Mascarenhas, R. Salgueiro, T. Silva, J. Correia, P.A. Carvalho, D. de Oliveira, Mechanochemical synthesis of tetrahedrite materials using mixtures of synthetic and ore samples collected in the Portuguese zone of the Iberian Pyrite Belt. Miner. Eng. **164**, 106833 (2021)
67. F.A. López Cota, J.A. Díaz-Guillén, O. Juan Dura, M.A. López de la Torre, J. Rodríguez-Hernández, A. Fernández Fuentes, Mechanosynthesis and thermoelectric properties of Fe, Zn, and Cd-Doped P-Type Tetrahedrite: $Cu_{12-x}M_xSb_4S_{13}$. Materials **14**, 3448 (2021)
68. D. Tetzlaff, K. Pellumbi, D.M. Baier, L. Hoof, H.S. Barkur, M. Smialkowski, et al., Sustainable and rapid preparation of nanosized Fe/Ni-pentlandite particles by mechanochemistry. Chem. Sci. **11**, 12835–12842 (2020)
69. M. Suyama, S. Yubuchi, M. Deguchi, A. Sakuda, M. Tatsumisago, A. Hayashi, Importance of Li-metal/sulfide electrolyte interphase ionic conductivity in suppressing short-circuiting of all-solid-state Li-metal batteries. J. Electrochem. Soc. **168**, 060542 (2021)
70. M. Tatsumisago, A. Hayashi, *Preparation of Solid Electrolyte Particles and Solid-Solid Interfaces for All-Solid-State Batteries*, Nanoparticle Technology Handbook (Elsevier, 2018), pp. 579–584
71. T. Kimura, A. Kato, C. Hotehama, A. Sakuda, A. Hayashi, M. Tatsumisago, Preparation and characterization of lithium ion conductive $Li_3SbS_4$ glass and glass-ceramic electrolytes. Solid State Ionics **333**, 45–49 (2019)
72. M. Otoyama, K. Kuratani, H. Kobayashi, Mechanochemical synthesis of air-stable hexagonal $Li_4SnS_4$-based solid electrolytes containing LiI and $Li_3PS_4$. RSC Adv. **11**, 38880–38888 (2021)
73. A. Nasu, M. Otoyama, A. Sakuda, A. Hayashi, M. Tatsumisago, Mechanochemical synthesis of cubic rocksalt $Na_2TiS_3$ as novel active materials for all-solid-state sodium secondary batteries. J. Ceram Soc. Jpn. **127**, 19086 (2019)

74. K.A. Ibrahimova, A.A. Azizov, O.O. Balayeva, R.M. Alosmanov, S.C. Mammadyarova, Mechanochemical synthesis of PbS/Ni–Cr layered double hydroxide nanocomposite. Mendeleev Commun. **31**, 100–103 (2021)
75. P. Baláž, M. Baláž, A. Zorkovská, I. Škorvánek, Z. Bujňáková, J. Trajić, Kinetics of solid-state synthesis of quaternary $Cu_2FeSnS_4$ (stannite) nanocrystals for solar energy applications. Acta Phys. Pol. A **131**, 1153–1155 (2017)
76. P. Baláž, M. Baláž, M.J. Sayagués, I. Škorvánek, A. Zorkovská, E. Dutková, et al., Mechanochemical solvent-free synthesis of quaternary semiconductor Cu-Fe-Sn-S nanocrystals. Nanoscale Res. Lett. **12**, 256 (2017)
77. P. Baláž, M. Baláž, M.J. Sayagués, A. Eliyas, N.G. Kostova, M. Kaňuchová, E. Dutková, A. Zorkovská, Chalcogenide quaternary $Cu_2FeSnS_4$ nanocrystals for solar cells: Explosive character of mechanochemical synthesis and environmental challenge. Crystals **7**, 367 (2017)
78. J. Trajic, M. Romcevic, N. Paunovic, M. Curcic, P. Balaz, N. Romcevic, Far-infrared study of the mechanochemically synthesized $Cu_2FeSnS_4$ (stannite) nanocrystals. Infrared Phys. Technol. **90**, 66–69 (2018)
79. J. Trajic, M. Romcevic, M. Petrovic, M. Gilic, P. Balaz, A. Zorkovska, N. Romcevic, Optical properties of the mechanochemically synthesized $Cu_2FeSnS_4$ (stannite) nanocrystals: Raman study. Opt. Mater. **75**, 314–318 (2018)
80. P. Baláž, M. Hegedus, M. Baláž, N. Daneu, P. Siffalovic, Z. Bujňáková, et al., Photovoltaic materials: $Cu_2ZnSnS_4$ (CZTS) nanocrystals synthesized via industrially scalable, green, one-step mechanochemical process. Prog. Photovolt. Res. Appl. **27**, 798–811 (2019)
81. E.M. Heppke, S. Mahadevan, T. Bredow, M. Lerch, Crystal structure of mechanochemically prepared $Ag_2FeGeS_4$. Z. Naturforsch., B: Chem Sci **76**, 607–614 (2021)
82. E.M. Heppke, S. Klenner, O. Janka, R. Pöttgen, M. Lerch, Mechanochemical synthesis of $Cu_2MgSn_3S_8$ and $Ag_2MgSn_3S_8$. Z. Anorg. Allg. Chem. **646**, 5–9 (2020)
83. F. Neves, A. Stark, N. Schell, M.J. Mendes, H. Aguas, E. Fortunato, R. Martins, J.B. Correia, A. Joyce, Investigation of single phase $Cu_2ZnSn_xSb_{1-x}S_4$ compounds processed by mechanochemical synthesis. Phys. Rev. Mater. **2**, 075404 (2018)
84. K. Kapusta, M. Drygas, J.F. Janik, Z. Olejniczak, New synthesis route to kesterite $Cu_2ZnSnS_4$ semiconductor nanocrystalline powders utilizing copper alloys and a high energy ball milling-assisted process. J. Mater. Res. Technol. **9**, 13320–13331 (2020)
85. K. Lejda, M. Drygaś, J.F. Janik, J. Szczytko, A. Twardowski, Z. Olejniczak, Magnetism of Kesterite $Cu_2ZnSnS_4$ semiconductor Nanopowders prepared by Mechanochemically assisted synthesis method. Materials **13**, 3487 (2020)
86. K. Tsuji, T. Maeda, T. Wada, Optical properties and electronic structures of $Cu_2ZnSnS_4$, $Cu_2ZnGeS_4$, and $Cu_2Zn$ (Ge, Sn) $S_4$ and $Cu_2Zn$ (Ge, Sn) $Se_4$ solid solutions. Jpn. J. Appl. Phys. **57**, 08RC21 (2018)
87. E.M. Heppke, S. Mahadevan, M. Lerch, New compounds of the $Li_2MSn_3S_8$ type. Z. Naturforsch., B: Chem Sci **75**, 625–631 (2020)
88. E.M. Heppke, M. Lerch, $Na_2MgSnS_4$–a new member of the A2IBIICIVX4 family of compounds. Z. Naturforsch., B: Chem Sci **75**, 721–726 (2020)
89. F. Tsuji, A. Nasu, A. Sakuda, M. Tatsumisago, A. Hayashi, Mechanochemical synthesis and characterization of $Na_{3-x}P_{1-x}W_xS_4$ solid electrolytes. J. Power Sources **506**, 230100 (2021)
90. F. Tsuji, N. Masuzawa, A. Sakuda, M. Tatsumisago, A. Hayashi, Preparation and characterization of cation-substituted $Na_3SbS_4$ solid electrolytes. ACS Appl. Energy Mater. **3**, 11706–11712 (2020)
91. R.P. Rao, X. Zhang, K.C. Phuah, S. Adams, Mechanochemical synthesis of fast sodium ion conductor $Na_{11}Sn_2PSe_{12}$ enables first sodium–selenium all-solid-state battery. J. Mater. Chem. A **7**, 20790–20798 (2019)
92. E. Gock, K.E. Kurrer, Eccentric vibratory mills-a new energy efficient way for pulverization. Erzmetall **49**, 434–442 (1996)
93. E. Gock, K. Kurrer, Eccentric vibratory mills – theory and practice. Powder Technol. **105**, 302–310 (1999)

94. M. Achimovicova, E. Dutkova, E. Tothova, Z. Bujnakova, J. Briancin, S. Kitazono, Structural and optical properties of nanostructured copper sulfide semiconductor synthesized in an industrial mill. Front. Chem. Sci. Eng. **13**, 164–170 (2019)
95. P. Balaz, M. Achimovicova, M. Balaz, K. Chen, O. Dobrozhan, E. Guilmeau, et al., Thermoelectric Cu-S-based materials synthesized via a scalable Mechanochemical process. ACS Sustain. Chem. Eng. **9**, 2003–2016 (2021)
96. P. Balaz, E. Guilmeau, M. Achimovicova, M. Balaz, N. Daneu, O. Dobrozhan, M. Kanuchova, Bismuth doping in nanostructured tetrahedrite: Scalable synthesis and thermoelectric performance. Nanomaterials **11**, 1386 (2021)
97. P. Baláž, M. Hegedüs, M. Achimovičová, M. Baláž, M. Tešinský, E. Dutková, M. Kaňuchová, J. Briančin, Semi-industrial green mechanochemical syntheses of solar cell absorbers based on quaternary sulfides. ACS Sustain. Chem. Eng. **6**, 2132–2141 (2018)
98. P. Baláž, M. Hegedüs, M. Reece, R.Z. Zhang, T.C. Su, I. Škorvánek, et al., Mechanochemistry for thermoelectrics: Nanobulk $Cu_6Fe_2SnS_8/Cu_2FeSnS_4$ composite synthesized in an industrial mill. J. Electron. Mater. **48**, 1846–1856 (2019)
99. M. Balaz, O. Dobrozhan, M. Tesinsky, R. Zhang, R. Dzunda, E. Dutkova, et al., Scalable and environmentally friendly mechanochemical synthesis of nanocrystalline rhodostannite ($Cu_2FeSn_3S_8$). Powder Technol. **388**, 192–200 (2021)
100. M. Hegedus, M. Achimovicova, H. Hui, G. Guelou, P. Lemoine, I. Fourati, et al., Promoted crystallisation and cationic ordering in thermoelectric $Cu_{26}V_2Sn_6S_{32}$ colusite by eccentric vibratory ball milling. Dalton Trans. **49**, 15828–15836 (2020)